JGR Biogeosciences

RESEARCH ARTICLE
10.1029/2022JG006895

Special Section:
Advances in scaling and modeling of land-atmosphere interactions

Quantifying the Natural Climate Solution Potential of Agricultural Systems by Combining Eddy Covariance and Remote Sensing

Susanne Wiesner[1,2], Ankur R. Desai[3], Alison J. Duff[4], Stefan Metzger[3,5], and Paul C. Stoy[2,3]

[1]Department of Plant and Earth Science, University of Wisconsin–River Falls, River Falls, WI, USA, [2]Department of Biological Systems Engineering, University of Wisconsin–Madison, Madison, WI, USA, [3]Department of Atmospheric and Oceanic Sciences, University of Wisconsin–Madison, Madison, WI, USA, [4]U.S. Dairy Forage Research Center, USDA Agricultural Research Service, Madison, WI, USA, [5]Battelle, National Ecological Observatory Network, Boulder, CO, USA

Abstract Livestock agriculture accounts for ~15% of global anthropogenic greenhouse gas (GHG) emissions. Recently, natural climate solutions (NCS) have been identified to mitigate farm-scale GHG emissions. Nevertheless, their impacts are difficult to quantify due to farm spatial heterogeneity and effort required to measure changes in carbon stocks. Remote sensing (RS) models are difficult to parameterize for heterogeneous agricultural landscapes. Eddy covariance (EC) in combination with novel techniques that quantitatively match source area variations could help update such vegetation-specific parameters while accounting for pronounced heterogeneity. We evaluate a plant physiological parameter, the maximum quantum yield (MQY), which is commonly used to calculate gross and net primary productivity in RS applications. RS models often rely on spatially invariable MQY, which leads to inconsistencies between RS and EC models. We evaluate if EC data improve RS models by updating crop specific MQYs to quantify agricultural GHG mitigation potentials. We assessed how farm harvest compared to annual sums of (a) RS without improvements, (b) EC results, and (c) EC-RS models. We then estimated emissions to calculate the annual GHG balance, including mitigation through plant carbon uptake. Our results indicate that EC-RS models significantly improved the prediction of crop yields. The EC model captures diurnal variations in carbon dynamics in contrast to RS models based on input limitations. A net zero GHG balance indicated that perennial vegetation mitigated over 60% of emissions while comprising 40% of the landscape. We conclude that the combination of RS and EC can improve the quantification of NCS in agroecosystems.

Plain Language Summary Animal farms like dairies are large greenhouse gas emitters globally, but opportunities exist to reduce these emissions by removing CO_2 from the atmosphere through plant biomass production. These opportunities have been termed natural climate solutions (NCS), but their efficiency has been difficult to estimate in ecosystems with mixed vegetation. Satellite remote sensing products can estimate plant biomass production, but they rely on simplified assumptions about plant biological functions like uniform photosynthetic efficiency across vegetation types. Approaches that measure differences in photosynthetic efficiency by plant vegetation types could improve these methods. We estimated plant photosynthetic efficiency and plant biomass productivity at the farm scale using instruments that measure the dynamic exchange of CO_2 between the land and atmosphere and incorporated that information into satellite remote sensing models. We then assessed which model predicted farm harvest best. We found that RS models that included local plant information predicted farm harvest best. Plant biomass production within the dairy farm offset annual greenhouse gas emissions, which was controlled by long-lived deep-rooted vegetation like forests and grasslands that took up the most CO_2. This study design has great potential to improve the assessment of NCS that offset greenhouse gas emissions in agricultural systems.

Key Points:

- Eddy covariance (EC) environmental response functions (ERF) allow for the upscaling of spatiotemporal carbon fluxes of mixed ecosystems
- EC ERF significantly improved remote sensing predictions of biomass harvests
- Dairy farms can mitigate all greenhouse gas emissions when one third of the vegetation is comprised of perennials like forests and grasslands

Supporting Information:

Supporting Information may be found in the online version of this article.

Correspondence to:

S. Wiesner,
susanne.wiesner@uwrf.edu

Citation:

Wiesner, S., Desai, A. R., Duff, A. J., Metzger, S., & Stoy, P. C. (2022). Quantifying the natural climate solution potential of agricultural systems by combining eddy covariance and remote sensing. *Journal of Geophysical Research: Biogeosciences*, *127*, e2022JG006895. https://doi.org/10.1029/2022JG006895

Received 8 MAR 2022
Accepted 30 AUG 2022

Author Contributions:

Conceptualization: Stefan Metzger
Data curation: Alison J. Duff
Funding acquisition: Alison J. Duff, Paul C. Stoy
Methodology: Ankur R. Desai, Stefan Metzger
Project Administration: Ankur R. Desai, Paul C. Stoy

1. Introduction

Atmospheric CO_2 concentrations are steadily increasing, with concentrations reaching 1.5 times preindustrial levels (Bloch-Johnson et al., 2021). Natural climate solutions (NCS, also termed nature-based climate solutions) that enhance biospheric carbon sinks and reduce or mitigate greenhouse gas emissions have been proposed to combat this climate crisis, demanding changes in ecosystem management (Griscom et al., 2017; Hemes et al., 2021). In the case of livestock agriculture, several "nature based" strategies have been identified to mitigate

Resources: Ankur R. Desai
Software: Stefan Metzger
Supervision: Ankur R. Desai, Stefan Metzger, Paul C. Stoy
Validation: Stefan Metzger
Writing – review & editing: Ankur R. Desai, Alison J. Duff, Stefan Metzger, Paul C. Stoy

on-farm greenhouse gas (GHG) emissions by imitating existing natural processes that sequester CO_2 from the atmosphere. These include cover crops (Bergtold et al., 2019; Blanco-Canqui et al., 2015; Chahal et al., 2020) and conversion of annual croplands to continuous green cover such as pastures or agroforestry (Bossio et al., 2020; Fargione et al., 2018; Griscom et al., 2017). However, evidence for mitigation capacities is variable, subject to high uncertainty, and often constrained by regional climate, soil type, management intensity, and ecosystem suitability (Bellamy & Osaka, 2020; Fleischman et al., 2020; Griscom et al., 2017).

While agricultural lands may be managed to offset farm originated GHG emissions, it is important to point out that these climate solutions are insufficient to fully mitigate GHG emissions (Anderson et al., 2019). For NCS to work it is vital to decrease GHG emissions from multiple sectors. To begin making informed decisions, it is important to establish baseline values to quantify NCS (Graves et al., 2020).

Calculation tools for agricultural GHG balances, here interpreted as net-zero CO_2-equivalent emissions (Fuglestvedt et al., 2018), often ignore the role that landscape productivity plays in whole-farm emission mitigation (Colomb et al., 2013; Wassmann et al., 2019). Livestock and cash crop agriculture typically involves management on multiple scales, including crop rotations, nutrient management, and barn activities. These decisions are nested within farm boundaries that interact with the surrounding landscape, including farm property that may be subject to active or passive GHG management (Leahy et al., 2020; Schwarze et al., 2002). These interactions, as well as the global warming potentials of different GHG emissions, impact the farm GHG balance and need to be considered for a complete understanding of farm-scale NCS (Paitan & Verburg, 2019; Styles et al., 2018). Measurements of such sources and sinks and their interactions are time consuming and often expensive, and hence rarely accessible to producers (Rosenstock et al., 2013). A broader suite of tools needs to be applied to successfully implement NCS in agricultural management and to track their success.

Satellite-based Earth observations are noninvasive, rapid, and can be free of charge—like Landsat and MODIS (Moderate Resolution Imaging Spectroradiometer)—and have the capacity to track changes in individual farm carbon balances based on management and land use changes (Anderson et al., 2018; Weiss et al., 2020; Wulder et al., 2019). While MODIS data have relatively low spatial resolution (250–1,000 m), Landsat imagery with its higher resolution (30 by 30 m) can better resolve field scales of typical agricultural farms. Remote sensing (RS) data have successfully predicted aboveground biomass with relatively low uncertainty in agricultural systems (Pique et al., 2020; Wiesner et al., 2020). However, their implementation into full farm GHG budgets is still limited (Sleeter et al., 2018). Furthermore, continuous breeding programs make it difficult to track changes in plant productivity, as plant physiological parameters change over time (Weiss et al., 2020). Such parameters include the maximum quantum yield (MQY; g C mol photons^{-1})—the carbon taken up per mol of photosynthetically active radiation (PAR) received—a key parameter in the quantification of gross primary productivity (Ogutu et al., 2013; Y. Zhang et al., 2017). MQY or other light use efficiency parameters are commonly used to calculate gross and net primary productivity (GPP and NPP) in RS applications (Joiner et al., 2018). RS models often rely on spatially invariable MQY, but differences in such parameters lead to inconsistencies between RS and eddy covariance (EC) models (Wang et al., 2020; Zhang et al., 2020). In the case of MODIS GPP and NPP products (MOD17 and MOD17A2/A3), a single MQY is assumed for crops (Running & Zhao, 2015; Running et al., 1999), thus introducing a substantial bias for the global estimation of agricultural yields. Studies found better correlations when separating out differences in MQY using EC approaches by plant functional types (i.e., C3 and C4) (Jiang et al., 2021). However, EC systems are expensive and require technical skills, and are often constrained to one vegetation type due to the basic assumptions underlying the measurement technique (Rafi et al., 2020; Sishodia et al., 2020), thus limiting their application range and accessibility.

Novel methods that quantitatively match EC source area variations (i.e., the "flux footprint") are being developed to overcome this limitation (Butterworth et al., 2021; Chu et al., 2021; Hannun et al., 2020; Helbig et al., 2021; Joy & Chávez, 2021; Metzger, 2018; Metzger et al., 2013; Xu et al., 2017). One of these techniques is the Environmental Response Function (ERF) approach by Metzger et al. (2013) and further improved by Metzger (2018) and Xu et al. (2017). The approach could be further refined to help update crop-specific parameters on a continuous basis by disaggregating the source area from which fluxes in heterogeneous landscapes arise. The ERF approach uses high frequency EC carbon and energy flux data and spatial information characterizing the landscape to account for differences in net ecosystem exchange (NEE) of CO_2 and other response variables based on variable footprint cover. The spatial information of surface-atmospheric exchange from different landcover types—as well as temporal meteorological drivers—is then used to build regression trees to assign carbon fluxes to biophysically

similar areas not covered by the footprint during the time interval in question. While this approach has been applied in previous studies to map gas fluxes across space and time, it had not been applied in agricultural systems and not over daily to annual time scales. Here we use the resulting spatiotemporal maps, among other things, to extract parameters like MQY for individual vegetation types, and update existing RS products (Huang et al., 2021; Xiao et al., 2004, 2010, 2012, 2019; Zhang et al., 2017), to better extrapolate carbon dynamics beyond individual farms.

Given these demands and advances, our research question thus arises: How reliably can we account for GHG mitigation approaches in heterogeneous agroecosystems through the combination of RS and EC technologies? To answer this, we use the US Dairy Forage Research Center (USDFRC) dairy farm in Wisconsin as a case study to (a) project NEE across space and time in a heterogeneous agricultural landscape using ERFs, and (b) understand how EC data from heterogeneous landcover types can inform RS measurements to scale NCS beyond the extent of an EC tower footprint. We use the data to improve the whole-farm GHG by improving the RS model parameter MQY using the ERF approach.

Our goal is to evaluate and provide tools for management recommendations that can increase carbon sequestration in agroecosystems and help quantify mitigation effects from NCS. We hypothesize that updating plant physiological parameters in RS models on a continuous basis using EC significantly improves NEE and yield estimations to quantify the GHG mitigation and economic potential of agricultural vegetation more accurately. To test this hypothesis, we used farm harvest records from the USDFRC farm to compare harvest yields to estimated yields from RS models without MQY improvements, from EC ERF results, and from improved RS models. The farm is uniquely positioned to perform such analyses as it is a working dairy farm but also serves research functions where changes in management to increase carbon sequestration and other ecosystem services can be tracked throughout the production chain.

2. Methods

In the following we describe how we apply ERFs and RS to estimate the spatiotemporal GHG balance of the USDFRC farm. First, we estimated daily timeseries of GPP and ecosystem respiration (R_{eco}) using MQY values from the literature for each crop and vegetation type to calculate net ecosystem productivity (NEP). Second, we used the EC ERF approach to obtain spatiotemporal maps of NEP. We then extracted NEP for each crop field (68 crop fields total) and the three perennial vegetation types (forest, shrubland, and grassland), resulting in 71 hourly NEP timeseries, which we used to calculate average MQY for each of the 10 vegetation types. We evaluated how different ranges of data affected yield estimation by calculating MQY using (a) all data, (b) only growing season data, and (c) only growing season daytime data. New MQY values were then used to recalculate RS NEP. Third, we calculated the total annual harvest NEP from harvest records using literature- and field-estimated root-to-shoot ratios (root:shoot) and dry matter data, as well as harvest indices (HI). Harvest NEP was then compared to annual sums of (a) RS NEP without improvements (RS_{Lit}), (b) ERF NEP, and (c) improved RS NEP (RS_{ERF}). Finally, we estimated farm emissions following Wiesner et al. (2020), to calculate the farm-scale GHG balance for 2019. Please refer to the Supporting Information S1 for a detailed description of emission calculations. We compare harvest biomass with estimated biomass from RS and EC models using NEP as the difference between carbon uptake through GPP and R_{eco}. We used this terminology as RS and EC quantify heterotrophic respiration in addition to autotrophic respiration. We assumed that harvest NPP approximated NEP, such that harvest biomass included C losses to microbial respiration from decaying biomass in form of leaves, roots, and stems over long periods of time (here 1 year).

2.1. Study Site

The study took place at the USDFRC farm located in Sauk County, Wisconsin USA. Mean annual temperature and annual precipitation are 8°C and 880 mm, respectively. Soils are moderately well drained to excessively drained. The USDFRC farm (~890 ha) houses approximately 350 dairy cows in both tie-stall and free-stall barns, in addition to 350 heifers and dry cows. Crops grown on the farm include corn for grain and silage, alfalfa for silage, soybeans, and winter wheat (Figure 1). The farm has hundreds of hectares of open pasture, grassland, shrubland and forest.

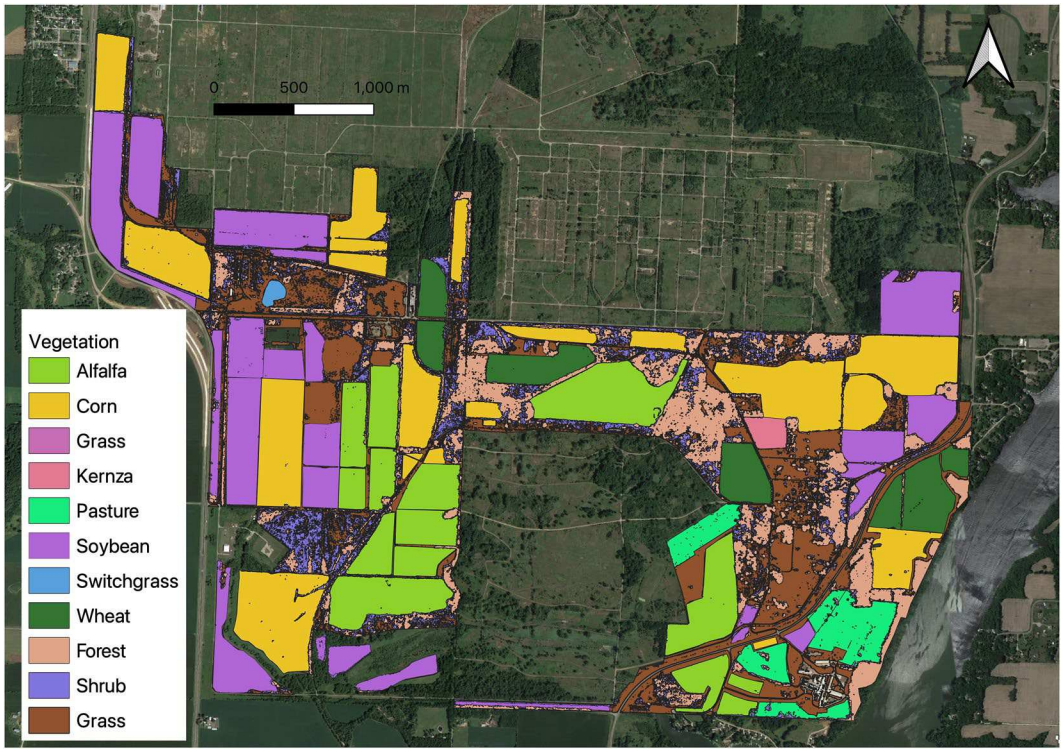

Figure 1. Crop and natural vegetation distribution at the U.S. Dairy Forage Research Center farm, Wisconsin, USA during 2019. IWG is intermediate wheatgrass (*Thinopyrum intermedium*). The red star indicates the location of the eddy covariance tower US-DFC. Black contour lines are the footprint climatology plotted with 10 percentile intervals; the outermost contour line shows the 90th percentile and the innermost shows the tenth percentile.

2.2. Remote Sensing Net Primary Productivity

We used Landsat 8 and MODIS (Aqua and Terra) data from 2019 to estimate gross ecosystem productivity (GPP; g C m^{-2}) using the Vegetation Photosynthesis Model (VPM, Xiao et al. (2004):

$$\mathrm{GPP}_{\mathrm{VPM}} = \varepsilon_g \times \mathrm{FPAR}_{\mathrm{chl}} \times \mathrm{PAR} \tag{1}$$

where $\mathrm{FPAR}_{\mathrm{chl}}$ is the fraction of daily sums of photosynthetically active radiation (PAR, mol d^{-1}) absorbed by chlorophyll calculated as $\mathrm{FPAR}_{\mathrm{chl}} = a \times \mathrm{EVI}$, where $a = 1$ (Xiao et al., 2004; Zhang et al., 2017), and EVI is the enhanced vegetation index. The light use efficiency ε_g is derived from the relationship of maximum quantum yield (MQY; g C mol^{-1} $photons^{-1}$; Table 1), initially assigned values taken from the literature ($\mathrm{Literature}_{\mathrm{MQY}}$) for each vegetation type (Madugundu et al., 2016), scalars of temperature (T_{scalar}) and vegetation water stressors (W_{scalar} and P_{scalar}) are:

$$\varepsilon_g = \mathrm{MQY} \times T_{\mathrm{scalar}} \times W_{\mathrm{scalar}} \times P_{\mathrm{scalar}} \tag{2}$$

where T_{scalar} ($0 < T_{\mathrm{scalar}} \leq 1$) is estimated as:

$$T_{\mathrm{scalar}} = \frac{(T - T_{\min})(T - T_{\max})}{(T - T_{\min})(T - T_{\max}) - (T - T_{\mathrm{opt}})^2} \tag{3}$$

where $T_{\min}$ (−1°C), $T_{\max}$ (48°C) and T_{opt} (30°C) are the minimum, maximum and optimum temperatures for photosynthetic activity for Wisconsin (Zhang et al., 2017) and T is satellite-measured land surface temperature (LST, °C). The term W_{scalar} ($0 < W_{\mathrm{scalar}} \leq 1$) is estimated as:

$$W_{\mathrm{scalar}} = \frac{(1 + \mathrm{LSWI})}{(1 + \mathrm{LSWI}_{\max})} \tag{4}$$

Table 1
Maximum Quantum Yield (MQY) Inputs for RS Models Using MQY From the Literature (RS_{Lit}), MQY Calculated From the Eddy Covariance Environmental Response Functions (ERF) Approach Using all Data ($ERF_{all,MQY}$), Growing Season Data Only ($ERF_{gs,MQY}$), and Growing Season Daytime Only (ERF_{MQY})

Crop	$Literature_{MQY}$ (g C mol PAR^{-1})	$ERF_{all,MQY}$ (g C mol PAR^{-1})	$ERF_{gs,MQY}$ (g C mol PAR^{-1})	ERF_{MQY} (g C mol PAR^{-1})
Alfalfa	0.60	1.03 (0.14)	0.51 (0.08)	0.55 (0.09)
Corn grain	0.69	0.68 (0.08)	0.51 (0.06)	0.65 (0.09)
Corn silage	0.69	0.58 (0.07)	0.53 (0.05)	0.50 (0.09)
Forest	0.56	0.23 (0.04)	0.36 (0.03)	0.23 (0.08)
Grass	0.75	0.82 (0.04)	0.86 (0.04)	0.86 (0.07)
Intermediate wheatgrass	0.75	0.70 (0.09)	0.38 (0.03)	0.46 (0.07)
Pasture	0.75	0.77 (0.09)	0.51 (0.03)	0.55 (0.08)
Shrub	0.30	0.89 (0.04)	0.77 (0.03)	0.65 (0.07)
Soybeans	0.39	0.67 (0.09)	0.44 (0.06)	0.64 (0.1)
Switchgrass	0.71	0.71 (0.06)	0.36 (0.04)	0.48 (0.08)
Wheat	0.80	0.70 (0.06)	0.34 (0.04)	0.52 (0.07)

Note. Numbers in parentheses show standard deviations by crop type. For literature MQY we did not include variability.

where $LSWI_{max}$ is the maximum land surface water index (LSWI) within the growing season, here prescribed as 0.78 from LSWI vegetation data for 2019. P_{scalar} ($0 < P_{scalar} \leq 1$) is estimated as:

$$P_{scalar} = \frac{(1 + LSWI)}{2} \quad (5)$$

Landsat 8 EVI (LC8EVI) and surface reflectance scenes (LC08L1TP, 16-day resolution) were downloaded from the USGS Earth Resources Observation and Science (EROS) Center Science Processing Architecture (ESPA). When Landsat scenes were not available, we used MODIS data to gapfill EVI, LST, and LSWI data as described below. MODIS surface reflectance (MOD09, MYD09), EVI (MOD13Q1, MYD13Q1) (Didan, 2015) and LST (MOD11A2, MYD11A2) (Wan et al., 2015) were downloaded using the NASA Earthdata AppEEARS API subsets tool (https://lpdaacsvc.cr.usgs.gov/appeears/); EVI was at 16-day resolution, and LST and surface reflectance to calculate LSWI was at 8 days. All Landsat and MODIS scenes were filtered using the respective quality assurance bands. Landsat and MODIS LSWI were estimated using the near and shortwave infrared bands via the *lswi* function from the 'water' package in R (Olmedo et al., 2016). Landsat LST was estimated by converting from brightness temperature following Sobrino et al. (2004). EVI, LST, and LSWI raster time series from Landsat were first gap-filled using linear interpolation between raster files from adjacent dates (within 16-day windows) via the *approxNA* function from the 'raster' R package (Hijmans, 2021). Landsat and MODIS EVI, LST, and LSWI were linearly interpolated to obtain daily satellite scenes for 2019. Because *approxNA* computes values for overlapping pixels between two dates, when one of the dates had missing values due to cloud cover or otherwise filtered data from QA bands, we gapfilled data using a linear regression between the Landsat and MODIS pixels of each respective day. MODIS data were first resampled using a bilinear interpolation to downscale from a resolution of 250 × 250 m pixels to 30 × 30 m pixels. While this may introduce biases based on overlapping vegetation types in single pixels, these should be small, as fields at the farm exceeded these scales on average by 100 times (ranging from 3 to 320 times the size of a single Landsat pixel).

Daily ecosystem respiration (R_{eco}) for the extent of the farm was estimated using RS GPP results, as well as satellite LST data, following Gao et al. (2015):

$$R_{eco} = a \times GPP + R_{ref} \times e^{E_0 \times \frac{1}{T_{ref} - T_0} - \frac{1}{LST - T_0}} \quad (6)$$

where E_0 is the temperature sensitivity of activation energy of respiration, estimated using the R package "ReddyProc" (Wutzler et al., 2018) using 2019 EC NEE data (Section 2.3). T_0 is the minimum temperature for respiration (°C), which was set to −46.02°C, following Lloyd and Taylor (1994) and T is Landsat/MODIS LST (°C).

The model estimates R_{eco} from autotrophic and heterotrophic respiration, using a constant fraction of GPP that is assumed to be spent on autotrophic plant respiration (here $a = 0.25$, following McCallum et al. (2009) and Waring et al. (1998)), and a reference respiration rate (R_{ref}), which was set to 2.86 g Cm^{-2} for a reference temperature of 10°C (T_{ref}), estimated from the Q_{10} relationship; the temperature sensitivity of EC respiration data to a 10°C increase in temperature. We obtained daily sums of NEP by subtracting RS R_{eco} from GPP (NEP = GPP − R_{eco}).

2.3. Eddy Covariance Data

A 30-m-tall EC tower was installed in April 2018. Instruments included a sonic anemometer (Gill New Windmaster, Lymington, Hampshire UK) and a 7500RS infrared gas analyzer (Licor Inc., Lincoln, NE, USA), measuring at 10 Hz. Meteorological sensors included air temperature and humidity (HMP155, Vaisala, Vantaa, Finland), global radiation (LI-200R, Licor Inc., Lincoln, NE, USA), and a net radiometer (CNR4, Kipp and Zonen, Delft, The Netherlands), recorded on a Sutron Xlite 9210 datalogger (Sterling, VA, USA) every 5 s and averaged to half-hours. Ground level sensors included a rainfall gauge (TR-525M, Texas Electronics, Dallas, TX, USA), three soil moisture and temperature sensors, and soil heatflux plates (Hukseflux HFP01), which were also connected to the datalogger. Biomet and flux files were automatically combined into .ghg files (a LI-COR custom raw file type, containing data and metadata information).

2.4. Environmental Response Function Approach

The Environmental Response Function (ERF) approach developed by Metzger et al. (2013) was first applied to flux towers by Xu et al. (2017) and involves three computational steps. First, high-frequency EC data is resolved using wavelet cross-scalograms to estimate NEE (μmol CO_2 m^{-2} s^{-1}). Here we estimated fluxes from the 10 Hz turbulence data using wavelet discretization for 10 min intervals, which were calculated using consecutive four-hour windows of 10 Hz raw EC data, to avoid edge effects (Xu et al., 2017). We used the Morlet wavelet with 1/8 resolution. Preprocessing of high frequency turbulence data involved de-spiking following Brock (1986) and Starkenburg et al. (2015), planar fit rotation (Wilczak et al., 2001), lag correction using maximum correlation, and conversion of sonic temperature to air temperature (Schotanus et al., 1983), as described in Metzger et al. (2013) and Xu et al. (2017). Turbulence data were screened according to EC quality assurance and quality control procedures, which included a steady-state test with a flag threshold of 100% (Foken & Wichura, 1996; Vickers & Mahrt, 1997) and an Integral Turbulence Characteristics test following Foken (2008). We corrected NEE for density fluctuations following Webb et al. (1980).

During the second step, a footprint algorithm quantified the contribution of different surfaces to NEE for each processing step (Kljun et al., 2004; Metzger et al., 2013). Boosted regression trees (BRTs) were estimated using wavelet results to build relationships between NEE, meteorological variables, and footprint-weighted surface properties (here, EVI and LST) to project hourly flux fields. BRTs were estimated using 30-day intervals with 10-min timesteps (N = 4,320), after which NEE responses were projected to the extent of the farm for hourly intervals. Thirty-day training intervals overlapped by 10 days each, to ensure the model was trained with intersecting data samples. Spatially-projected fluxes were based on EVI and LST pixel resolution, yielding a spatiotemporal resolution of hourly 30 by 30-m grids. We included air temperature (°C), the mole fraction of water vapor in dry air (mol mol^{-1}), and incoming solar radiation (W m^{-2}), all measured at the tower, as well as solar azimuth (degree), daily EVI (unitless), and daily land surface temperature (K) from Landsat data in the ERF algorithm. Solar azimuth was used to describe the diurnal cycle and was calculated using *sunAngle* from the 'oce' package (D. E. Kelley, 2018; D. Kelley & Richards, 2021) in R. Surface properties (EVI and LST) were used to explain the spatial variability (and similarities among vegetation type) of the response, while meteorological drivers were used to explain the diurnal cycle and temporal variability. We focused on these variables as main drivers of NEE through photosynthesis and autotrophic and heterotrophic respiration (via radiation, temperature, and water availability), while maximizing the number of observations, tree complexity and number of regressions trees to compute final fluxes, as we were limited to 30-day intervals of 10 min data due to the computational restrictions of the CyVerse environment (16 GB RAM) and RStudio. During projection, hourly medians of the meteorological drivers were used which were assumed to be homogeneous across the farm. Please visit https://zenodo.org/record/6772181 for more information on driver-response relationships (equidistant response-sensitivity plots) that were the result of model training and validation. Random and systematic uncertainty was quantified using the mean absolute deviation following Xu et al. (2017) except for the ERF projection

performance analysis. All model uncertainties were incorporated into the ERF uncertainty budget as described in Section 2.7. All computations were performed in RStudio on the CyVerse servers.

Once applied, we extracted NEE from all crop fields ($N = 68$ crop fields total, including one intermediate wheatgrass field and five pastures) and three natural vegetation types (grasslands, shrublands, and forest, $N = 3$) using polygon shapefiles supplied by the farm using the *extract* function in the "raster" package in R. We extracted the mean and standard deviation of NEE for each polygon. All 71 NEE hourly time series were then filtered and gap-filled following typical EC processing procedures using REddyProc and micrometeorological data collected at the EC tower. Because RS model input data were daytime only, we compared gapfilled average daytime ERF data ($Rs > 10$ W m^{-2}) for each crop field and vegetation type and converted to daily sums of NEP (g C m^{-2}), which resulted in a better fit between the two timeseries. For the comparison of annual NEP from harvest, RS models, and ERF NEP, we assumed that—NEE from ERF approximates NEP in the crop fields on an annual basis, as the cumulative, total difference between all CO_2 sources and sinks within the entire system (Teets et al., 2018). To quantify ERF performance, we compared ERF NEE hourly fluxes from fields around the US-DFC tower, as well as fields outside of the US-DFC tower footprint, to a nearby EC tower, located in the intermediate wheatgrass (IWG) field (US-DFK, Wiesner et al., 2022). We compared ERF time series of different crops (IWG, pasture, forest, soybeans, corn, and alfalfa) to the US-DFK time series to estimate how well ERF predicted NEE fluxes of IWG. To understand how well hourly and monthly average daily NEE time series corresponded, we determined the mean absolute percent error (MAPE), Pearson correlation coefficient (r), and the dynamic time warping Euclidian distance (DTW_d) between gapfilled and non-gapfilled time series of the US-DFK tower and ERF time-series consisting of IWG, soybeans, corn, alfalfa, pasture, and forest. DTW_d was used to understand similarity among time series (Baek et al., 2021; Bellman & Kalaba, 1959), which was computed using the function *dtw* from the package "dtw" in R (Giorgino, 2009).

2.5. Harvest NPP and Aboveground and Belowground Biomass Collections

Crop harvests occurred between June and November 2019, with four alfalfa harvests throughout the growing season until September, corn silage harvest in September, soybean and high moisture corn harvests in October, dry corn harvest in November, and winter wheat in late July. Winter wheat yields were estimated from harvest load weights and assigned to fields proportionally based on acreage and historical yield data. Harvest biomass was weighed and stored on site, except for winter wheat harvests, 53% of dry corn kernels, and 22% of soybean harvests, which were sold (Table 3). We used harvest index data (HI; established from personal conversation with the farm manager; Wiesner et al., 2020), dry matter fractions (Table S1 in Supporting Information S1), and root to shoot ratios from the literature (Agostini et al., 2015; Bolinder et al., 2007; IPCC, 2006; Little et al., 2017; Saggar et al., 2015) to calculate $NEP_{Harvest}$. To check whether literature values for root:shoot and dry matter mass would bias our results, we calculated harvest NEP using data from a 2019 field campaign, where aboveground and belowground biomass were collected at three different time points during 2019 (May, July and September). Aboveground and belowground biomass was collected at three randomly distributed locations from the 26 crop fields within the EC tower footprint using 0.5 × 0.5 m quadrats. Vegetation types included alfalfa (3 fields), intermediate wheatgrass (1 field), soybeans (8 fields), corn grain (4 fields) and silage (2 fields), wheat (3 fields), and pasture (5 fields). All biomass within the quadrats was harvested flush with the quadrat frame and then oven dried at 60°C for a minimum of 36 hr or until dry weights had stabilized before recording biomass. Belowground biomass was estimated using soil cores after aboveground biomass was harvested from 0 to 10, 10–20, 20–40, and 40–60 cm (soil core radius of 1.5 cm), where 10 cm cores had a volume of 70 cm^3 and 20 cm cores had a volume of 140 cm^3. Soil cores were washed, and roots were extracted, dried, and weighed. We converted belowground biomass to g m^{-2} using the sum of dry matter fractions for each soil layer and a bulk density of 1.5 g m^{-3}, representing an average for the farm soils. Total field harvest biomass was converted to g C using a conversion factor of 450 g C per kg biomass (IPCC, 2006). To quantify how well RS models and ERF predicted annual field NEP we used linear zero intercept models to quantify the slope and adjusted coefficient of determination (R^2). We also estimated the Nash-Sutcliffe efficiency to understand the fit of predicted and estimated harvest biomass (Krause et al., 2005).

2.6. Maximum Quantum Yield Improvements

We used ERF results to update MQY values for the different crops (i.e., alfalfa, wheat, soybeans, corn grain and corn silage, Table 1) and perennial vegetation types (i.e., pasture, shrublands, forest, grasslands, and intermediate

wheatgrass). To obtain MQY we fitted light response curves using NEE, R_{eco}, and photosynthetically active radiation (PAR) converted from global radiation measured at the eddy covariance (EC) tower using the Rg.to.PPFD function of the "bigleaf" package in R (Knauer et al., 2018). We quantified MQY in three different ways, using (a) all hourly ERF NEE data ($ERF_{all,MQY}$) as input to the RS model ($RS_{ERF,all}$), (b) hourly ERF NEE data from the May to October growing season only ($ERF_{gs,MQY}$) to run the RS model ($RS_{ERF,gs}$), and (c) hourly ERF NEE daytime data (hours 10:00 a.m–3:00 p.m local time) from the growing season only (ERF_{MQY}) to replace literature MQY in the RS models (RS_{ERF}). We selected that timeframe to match Landsat 8 (11 a.m. Central Daylight Time, CDT) and MODIS (noon to 2 p.m. CDT) collection times within one hour. ERF_{MQY} was calculated for each month for each field and vegetation type and an average value was selected as the final MQY for each vegetation. We used the ERF MQY values as inputs to the RS GPP and R_{eco} models to evaluate if the new RS NEP estimates improved the prediction of farm harvest. We used Pearson correlation analysis and linear models to understand how well RS and ERF time series correspond.

2.7. Uncertainty Analysis

Annual uncertainty of RS NEP was estimated by propagating daily GPP and R_{eco} standard deviations for each field. Annual and daily ERF NEP uncertainty was propagated from ERF random and systematic model uncertainty, systematic and random gapfilling uncertainty, as well as from field extracted standard deviations. Harvest NEP uncertainty was accounted for by propagating the root:shoot uncertainty. Uncertainty of HI was assumed to be negligible, based on communication with the farm manager, as well as findings from other studies which showed low variability in HI from the Midwestern US (Prince et al., 2001).

Cattle diet nutrient intake and volatile solid output uncertainties were estimated using nutrient variations from laboratory analyses of forage for (crude protein) CP, ash, ether extract (EE), and neutral detergent fiber (NDF) and propagated to emission calculations. We also included standard deviations for feed dry matter (for enteric CO_2) and gross energy (for enteric CH_4) intakes and body weights for each cattle group. For direct N_2O emissions we also incorporated suggested uncertainties of ±50% from IPCC reports. For volatile manure N_2O emissions we varied the fraction of volatile gas for manure from 15% to 60% as suggested by IPCC (IPCC, 2006). We varied the fraction of leaching by ±10% for *N* losses from manure pit leaching (Syswerda et al., 2012). For each calculation step we estimated the percent variability which was then propagated to the next calculation step and finally to the parameter of interest for each day and for the year. Finally, uncertainties for C milk exports were estimated from fat, protein and milk energy content variations taken from milk test day results from 2019. Uncertainties for diesel emissions, electricity and natural gas consumption were assumed to be low as purchase records were available.

3. Results

3.1. Annual Harvest Yields and Spatiotemporal Net Ecosystem Production of Carbon

Annual farm harvest data indicated the greatest total biomass production from corn and alfalfa fields. However, total biomass varied as a function of literature ($Harvest_{Lit}$) or field ($Harvest_{Field}$) measured root:shoot and dry matter percentages (Table S1 in Supporting Information S1). From farm data alone the USDFRC dairy farm accumulated between 13 and 15 million kg of CO_2, where approximately 3 million kg of CO_2 were sold and exported from the farm boundaries. Overall, uncertainty arising from root:shoot and dry matter values from farm harvest data was greater (by up to 500%) compared to RS and ERF uncertainties combined (Figure 2).

3.2. Remote Sensing of the Net Ecosystem Production of Carbon

RS_{Lit} predicted field NEP well (an overestimation of $Harvest_{Lit}$ and $Harvest_{Field}$ by 11%–19%), however R^2 and Nash-Sutcliffe (E_f) values were lower (R^2 = 0.86 and E_f = 0.57) compared to ERF (0.89 and 0.62) and RS_{ERF} (0.89 and 0.68, Figure 2). ERF overestimated field $Harvest_{Lit}$ and $Harvest_{Field}$ by 13%–20%, but the variance of predicted versus $Harvest_{Lit}$ and $Harvest_{Field}$ was lower compared to RS_{Lit} (standard error 0.056 vs. 0.049; Figure 2). RS_{ERF} predicted $Harvest_{Lit}$ and $Harvest_{Field}$ within a 5% error margin. Overall, RS_{ERF} results improved the model fit (slope and R^2, Figure 3) by 10%–17%, depending on the harvest NEP model (e.g., field root:shoot). RS results using ERF_{all} MQY ($RS_{ERF,all}$) data resulted in an overprediction of total crop yield by ~27–35% (E_f = 0.36), whereas $RS_{ERF,gs}$ underestimated crop yield by 13%–29% (E_f = 0.62), depending on the harvest biometric model (Figure S2 in Supporting Information S1).

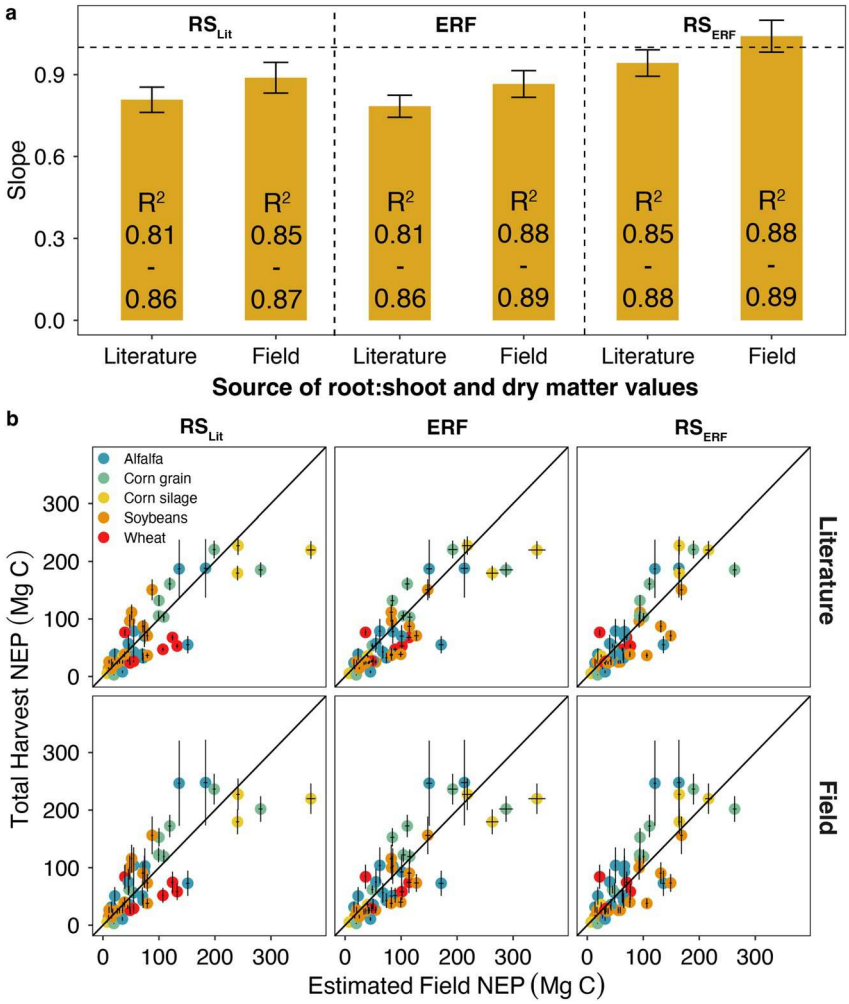

Figure 2. Regression results (a) calculated for net primary productivity results from remote sensing (RS) models using maximum quantum yield (MQY) data from the literature (RS_{Lit}), eddy covariance Environmental Response function (ERF) results (ERF) and improved RS models using ERF MQY calculated from growing season daytime data (RS_{ERF}) versus harvest data using literature measured root:shoot and dry matter values (Literature) and field sourced root:shoot and dry matter values (Field), and (b) comparison of total net primary productivity (NPP) from harvest data using literature root:shoot and dry matter values and field-measured root:shoot and dry matter values, with eddy covariance ERF and RS models RS_{Lit}, ERF, RS_{ERF}. Error bars indicate variability associated with uncertainties from each respective model.

Estimated farm NEP using literature MQY in RS models (RS_{Lit}) yielded similar results to the ERF approach, whereas the improved models using ERF_{MQY} (RS_{ERF}) yielded overall lower biomass, except for soybeans (Table 2). RS models using $ERF_{all,MQY}$ ($RS_{ERF,all}$) predicted the greatest NEP for all vegetation types. In contrast, total annual NEP from RS models using $ERF_{gs,MQY}$ ($RS_{ERF,gs}$) yielded overall lower estimates for each crop type.

Harvest predictions using RS models improved for all crop types using ERF_{MQY}, except for soybeans ($E_f = 0.36$), which showed a better fit when using $ERF_{gs,MQY}$ that included both daytime and nighttime information ($E_f = 0.57$; Figure S1 in Supporting Information S1). Our data also indicated that MQY was different for corn silage (0.5; $E_f = 0.9$) and corn grain (0.65; $E_f = 0.69$) varieties grown at the farm. Overall corn yield prediction was subject to the lowest uncertainty ($R^2 > 0.9$) compared to other crops. Alfalfa harvest models correlated better with RS results when using literature root:shoot (slope = 0.99; $E_f = 0.6$ vs. 0.49 for field root:shoot), while ERF corresponded better with alfalfa $Harvest_{Field}$ when using greater root:shoot (slope = 1; $E_f = 0.61$ vs. 0.42 for literature root:shoot; Figure S1 in Supporting Information S1). Similarly, our data indicated a close correlation of predicted yields from RS and ERF for wheat when using field measured root:shoot ratios ($Harvest_{Field}$). Nevertheless, the fit was lowest for wheat models compared to other crop types at the farm ($E_f < 0$ for all models).

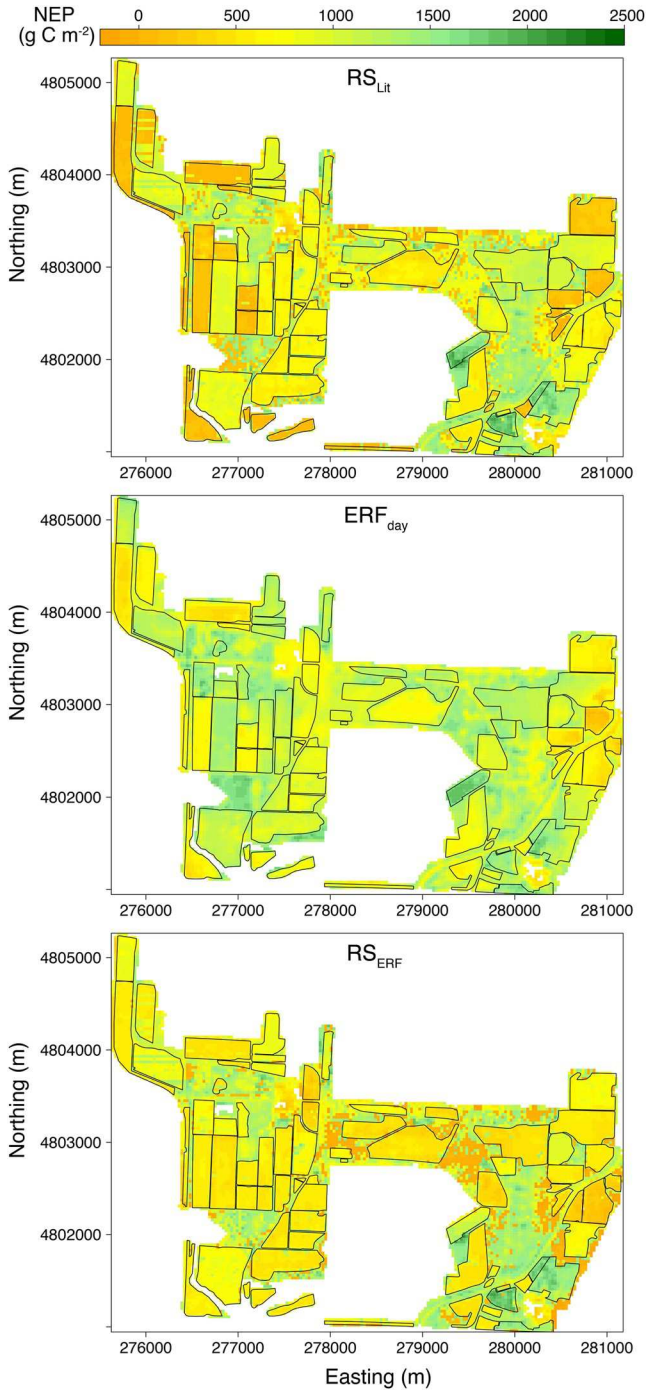

Figure 3. Total annual farm net ecosystem productivity (NEP) from remote sensing models which used maximum quantum yield (MQY) values from the literature (RS_{Lit}), daytime NEP eddy covariance data calculated using the environmental response function approach (ERF_{day}), and remote sensing models which used MQY values from growing season daytime data (RS_{ERF}).

Perennial vegetation types (forest, grasslands, and shrublands), as well as pastures and the intermediate wheatgrass (IWG) field accounted for over 55%–60% (depending on MQY) of total accumulated CO_2 at the USDFRC farm, with grasslands and forests taking up the most carbon per year. RS_{Lit} estimated lower total annual yields compared to ERF which yielded NEP values amounting to 55% of the total CO_2 taken up by the USDFRC vegetation (Figure 4, Table 2). RS_{ERF} predicted greater yield for all perennial vegetation types, except for forests and IWG. $RS_{ERF,all}$ and $RS_{ERF,gs}$ yielded similar values for perennial vegetation types. Overall, annual NEP from RS_{Lit} and corresponded best with ERF, $RS_{ERF,gs}$ and RS_{ERF} (Figure 4, Table 2).

All approaches revealed lower annual productivity for soybean fields (Figure 3, trending to more orange shades below 500 g C m^{-2}). Alfalfa fields also had relatively low annual NEP, ranging from 500 to 1,000 g C m^{-2}. The greatest annual NEP (>1,500 g C m^{-2}) was observed in grasslands and pastures, whereas forest and shrubland NEP was below 1,000 g C m^{-2}. Projections of annual daytime NEP from ERF for the intermediate wheatgrass field were >1,000 g C m^{-2} (Figures 3 and 4).

3.3. Annual Farm Net Ecosystem Exchange of Carbon From Eddy Covariance Data

Total annual NEE including daytime and nighttime EC ERF results also showed that soybean and older alfalfa fields (>2 years) tended to lose C on an annual basis (100–200 g C m^{-2}; blue shades on Figure 5), whereas corn fields, and other crop fields remained at a positive field carbon balance (brown shades), while having an overall lower annual NEE balance compared to natural perennial vegetation types (forests, grasslands and shrublands). Total ERF NEE results suggested a positive annual NEE balance for all natural perennial vegetation types (~100–400 g C m^{-2}). Projections of total annual ERF NEE for the IWG field were between 300 and 400 g C m^{-2} (Figure 5). Total annual NEE (daytime and nighttime) was greater for forests compared to grasslands. ERF NEE estimates for perennial vegetation had overall lower total uncertainty compared to annual crops.

For NEE time series comparisons with a nearby EC tower (US-DFK) located in an intermediate wheatgrass field, we found that hourly and monthly averages of NEE corresponded best with the IWG ERF NEE time series (Figure S3 in Supporting Information S1). While the ERF NEE time series for the nearby alfalfa field (4,450) showed lower MAPE (4.0) and a greater correlation coefficient (0.86) compared to IWG (4.6 and 0.77), the DTW distance (DTW_d) indicated a better fit with IWG, than alfalfa (27,956 vs. 30,744, respectively). Other vegetation types showed greater MAPE (>4.6), lower correlation coefficients ($0.45 \leq r \leq 0.7$), and greater DTW_d compared to IWG (>28,000), except for the pasture field 4,300, which showed slightly lower DTW_d (27,715). For fields outside of the average 90% EC footprint, MAPE increased up to 8 and r was reduced to as low as 0.59. DTW_d of fields from outside of the footprint increased up to 32,586.

3.4. Emission Estimates

Total farm emissions (~0.64 Gg ± 0.04 CO_2-eq $month^{-1}$; ~9.9 ± 0.7 Gg per year; Table 3) were driven by enteric fermentation, with dairy cows being the main contributors based on their numbers and the amount of feed they ingested (Figure 6). Greater overall emissions during summer months resulted from low spreading activity and greater manure pit emissions due to higher monthly air temperatures (>20°C). Similarly manure N_2O emissions were largest during spring, summer,

Table 2
Net Ecosystem Productivity (NEP, Gg of CO_2) From Remote Sensing (RS) Models Calculated Using Literature Values (RS_{Lit}), the Eddy Covariance Environmental Response Function Approach (ERF), NEP Data From RS Models Calculated Using ERF Maximum Quantum Yield From Growing Season Daytime Data (RS_{ERF}), all Eddy Covariance ERF Data ($RS_{ERF,all}$), and Growing Season Data Only (RS_{ERFgs})

Crop	RS_{Lit} (Mg of C)	ERF (Mg of C)	RS_{ERF} (Mg of C)	$RS_{ERF,all}$ (Mg of C)	$RS_{ERF,gs}$ (Mg of C)
Alfalfa	1,036.4	1,200.0	927.3	2,018.2	845.5
Corn grain	1,200.0	1,200.0	1,145.5	1,200.0	872.7
Corn silage	900.0	763.6	572.7	763.6	545.5
Soybeans	763.6	1,390.9	1,309.1	1,390.9	872.7
Wheat	518.2	436.4	272.7	436.4	163.6
Forest	1,363.6	1,554.5	1,009.1	1,281.8	1,009.1
Grasslands	2,727.3	2,918.2	3,545.5	3,545.5	3,545.5
Pastures	49.1	463.6	545.5	572.7	572.7
Shrublands	272.7	1,090.9	1,145.5	1,254.5	1,172.7
IWG	49.1	54.5	35.5	40.9	38.2

and early fall months, when the manure pit was either agitated for spreading (spring and fall) or temperatures increased above 20°C (summer). Total emissions slightly decreased in September because more dairy cows transitioned to dry stalls (Figure 6). As a result, total feed intake and manure excretion decreased temporarily.

3.5. Net Farm Carbon Balance

Daily and annual sums of NEP from ERF were less than 0.5 of RS_{Lit} (correlation ~0.76; Figure 7). However, we found that RS_{Lit} and RS_{ERF} showed good agreement with daytime ERF data (Rg > 5 W m^{-2}; slope = 0.88–0.92; correlation ~0.9, Figure 7, ERF_{day}). RS models predicted more respiration during winter (December–February) compared to ERF, which predicted negligible respiration.

The farm mitigated all barnyard (Figure 6) and management (diesel, gas, etc.) emissions (~9.88 Gg of CO_2eq), as well as feed refusal (0.2 Gg of CO_2eq) and milk exports (0.05 Gg CO_2), when comparing to ERF CO_2 uptake results for the year 2019 (10.6 Gg of CO_2). However, when we accounted for harvest exports (3 Gg of CO_2eq; Table 3) the farm exceeded net zero by 2.6 Gg of CO_2eq. The most vulnerable days for GHG mitigation were during the shoulder seasons (March and November), when plant CO_2 uptake was low, especially for fields with annual crop species and high manure spreading activity (i.e., soybeans).

4. Discussion

4.1. Net Ecosystem Carbon Balance of the USDFRC Farm

Farm emissions, which included enteric fermentation, emissions from the manure pit, and field applications were mitigated by on-farm crop production and perennial natural vegetation (i.e., forests, shrublands, grasslands and pastures). Perennial natural vegetation, while comprising only 40% of the farm area, mitigated ~60% of farm emissions. Our results are in support of commonly identified NCS to mitigate GHG emissions, which include high carbon accumulation capacity of pasture ecosystems with conservative nutrient management (Fargione et al., 2018; Griscom et al., 2017; Voglmeier et al., 2020; Wall et al., 2020). Increasing pasturing in dairy cattle production systems often increases enteric fermentation while also reducing milk efficiency (Beukes et al., 2010), but several studies found overall lower GHG budgets of dairy farms that had greater proportions of pastures on farm (Ribeiro-Filho et al., 2020) due to lower agricultural intensity.

Peaks of low emission mitigation capacity occurred during shoulder seasons (November through mid-May), when plant CO_2 uptake was low, especially for winter fallow fields. We observed the lowest emission mitigation capacity for the months of February, May, and October, due to low temperatures and snow cover (February), as well as frequent manure spreading, planting and harvest activities (May, October) leading to greater field N_2O, CH_4, and CO_2 emissions. Emission mitigation potential increased again in March, presumably due to snow melting and initiating plant activity from perennial natural vegetation (Lubbe et al., 2021; Vyse et al., 2019). Maximum mitigation potential was observed in July and August when plant productivity was at its peak.

While other research has identified increased feed efficiency as an approach that would reduce GHG emissions in dairy farms (Jayasundara et al., 2019), our data suggest that improving landscape productivity via perennial vegetation and reducing winter fallow would allow for more realistic mitigation strategies. While NCS such as the implementation of agroforestry and pastures (Fargione et al., 2018; Griscom et al., 2017) in integrated livestock systems may reduce plant productivity at the field scale and feed efficiency at the animal level, the increased C sequestration capacity of these solutions could substantially reduce (via lower input requirements) and/or mitigate (via greater production) on-farm GHG emissions from cattle.

Table 3
Annual Harvest Calculated Using Literature Root:Shoot Ratios ($Harvest_{Lit}$) and Farm Measured Root:Shoot Ratios ($Harvest_{Field}$) and Estimated Net Ecosystem Productivity (NEP) From Total Annual Eddy Covariance Environmental Response Function Results (ERF), Daytime ERF Data (ERF_{day}), Remote Sensing Models Using Literature Data (RS_{Lit}) and Improved Remote Sensing Models (RS_{ERF}), as Well as Barnyard and Management Emissions and Exports in CO_2eq at the Dairy Forage Research Center Farm for 2019

Type	Whole farm (Gg CO_2)	Natural vegetation (Gg CO_2)	Crop fields (Gg CO_2)
NEP ERF	10.6 (0.39)	6.8 (0.25)	3.8 (0.14)
NEP ERF_{day}	40.3 (1.49)	22.0 (0.81)	18.3 (0.68)
NEP RS_{Lit}	40.4 (0.77)	20.1 (0.38)	16.5 (0.31)
NEP RS_{ERF}	38.8 (0.70)	19.1 (0.35)	15.8 (0.29)
$Harvest_{Lit}$	--	--	13.3 (1.8)
$Harvest_{Field}$	--	--	15.0 (2.0)
Harvest export	--	--	3.11 (0.4)
Diesel	0.36 (−)	--	--
Natural gas	0.13 (−)	--	--
Electricity	0.03 (−)	--	--
Milk export	0.05 (0.009)	--	--
Feed refusal export	0.2 (0.003)		
Enteric methane	2.4 (0.007)	--	--
Enteric CO_2	3.3 (0.01)	--	--
Manure CH_4	0.7 (0.008)	--	--
Barn floor CO_2	0.9 (0.007)	--	--
Barn floor CH_4	0.15 (0.001)	--	--
Barn floor NH_3	0.02 (<0.001)		
Manure N_2O	0.06 (0.001)	--	--
Manure N_2O vol	0.7 (0.7)	--	--
Manure NH_3 vol	0.3 (<0.001)	--	--
Manure N_2O leach	0.1 (0.01)	--	--
Field manure & fertilizer	0.62 (0.003)	--	--
Urea	0.11 (0.002)	--	--

Note. Numbers in parentheses show uncertainties estimated as described in Section 2.7.

4.2. Remote Sensing Model Improvements Using Eddy Covariance

We show that EC CO_2 exchange can be extended beyond the EC footprint to the farm scale using the ERF approach developed by Metzger et al. (2013) and Xu et al. (2017), as evidenced by good agreement with harvest data. Updating plant physiological parameters such as MQY in RS models using EC ERF significantly improved the prediction of crop yields ($Harvest_{Lit}$ and $Harvest_{Field}$) for crops grown at the farm. While RS_{Lit} showed good agreement with $Harvest_{Lit}$ and $Harvest_{Field}$, ERF inputs decreased the spread of data variability and improved the overall fit by ∼10%. An improvement of this magnitude is promising for more accurate predictions of changes in carbon stocks within agricultural production systems beyond the boundaries of one farm. Using Landsat data this could be accomplished on field to regional scales, similar to other RS products (Xue et al., 2021). While other studies achieved similar results using data-model fusion techniques, their results are often based on single towers for individual landcover types (Chen et al., 2010; Fu et al., 2014). Our approach uses a single tower for multiple vegetation types, thereby improving the cost efficiency compared to multi-tower operations (Novick et al., 2022).

We showed that EC ERF can extend the scale of EC footprints to a farm and landscape level, thus matching the scale of RS models. All 10 vegetation types from a single 30 m eddy-covariance tower ($N = 1$) could be quantified separately by ERF, where traditional eddy-covariance would require at least one tower per vegetation type ($N = 10$). This improves the economic viability of eddy-covariance by an order of magnitude when linked to RS via ERF. It further makes the integrated data product more robust through exact spatial matching of the inputs and by quantifying variability within each vegetation type. Hence, strategically placed EC towers within agricultural regions could serve as benchmark sites to inform RS parameters to map landscape productivity and agricultural yields beyond single farms on regional or national scales (Smith et al., 2019), in addition to obtaining more fine scale information on CO_2 exchange of the landscape. Furthermore, such benchmark sites would allow for automated MQY value calculations that could be used as input to regional RS products (Running & Zhao, 2015; Running et al., 1999; Wang et al., 2020), to account for the spatial and temporal variability of different vegetation types. These models could then be used to estimate changes in ecosystem C accumulation on regional or national scales by quantifying the interannual variability of C inputs and exports, as a function of harvest exports and crop residues. More importantly, trends in changing plant physiological parameters due to climate change (i.e., rising CO_2 and air temperatures) could be implemented in predictions of future crop yields to understand the suitability and profitability of certain cropping systems while accounting for physiological adaptations to higher temperatures and atmospheric CO_2 concentrations (Dusenge et al., 2019). Accounting for these changes over time rather than relying on average MQY data from the literature could substantially improve future predictions of carbon stocks and crop yields (Crous, 2019). This is crucial as crops are being improved by plant breeders on a continuous basis (Hickey et al., 2019), or are subject to changes in chemical applications (Shao et al., 2013) resulting in plant physiological changes (Dusenge et al., 2019; Meena et al., 2021), which are often ignored in RS applications that estimate gross primary productivity due to their large spatial and temporal variability (Xu et al., 2020).

Data assimilation approaches described here can inform regional and global models on a continuous basis to improve accuracy of agricultural carbon and GHG budgets as they evolve over time (Smith et al., 2019). This is especially important with growing ecosystem service markets that often rely on sparse sampling and oversimplified RS models to predict soil carbon changes, thereby likely over- or underestimating true changes in carbon stocks (Bowen & Wittneben, 2011; Olander et al., 2013). For example, a recent study found that the spatial

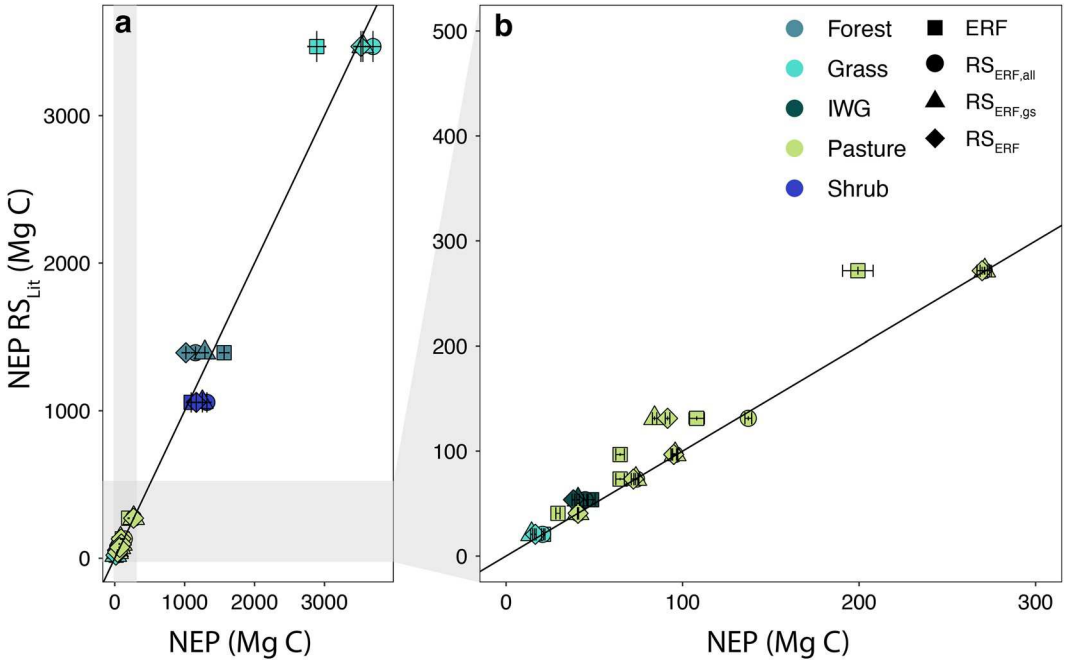

Figure 4. Comparison of total annual net ecosystem productivity (NEP, Mg C) for perennial vegetation types (forest, grass, intermediate wheatgrass [IWG], pasture and shrub) from remote sensing (RS) models using literature maximum quantum (MQY) yield data (RS_{Lit}) versus annual eddy covariance results using the environmental response function approach (ERF), as well as NEP results and RS models with MQY using all eddy covariance data ($RS_{ERF,all}$), growing season data ($RS_{ERF,gs}$), growing season daytime data (RS_{ERF}). Panel (a) represents all data, while panel (b) is zoomed in to 0–500 Mg C of Field NEP RS_{Lit} and 0–300 Mg C of ERF NEP, to highlight differences for pasture locations, grassland, and IWG.

landscape configuration and landscape processes (i.e., edge effects, field size, etc.) have been underrepresented in the quantification of ecosystem services to date (Metzger et al., 2021).

The EC-ERF-RS approach presented here could account for these interactive processes to estimate carbon, water, and energy exchanges at the landscape scale, while substantially reducing the uncertainty around these estimates. Additionally, our approach can be used to quantify the effect size of NCS in crop-livestock systems, including adoption of cover crops and conversions to grazing pastures (Graves et al., 2020), by establishing baseline estimates of landscape productivity. Following the establishment of baseline C dynamics, the effect size of NCS at the field or farm scale could be used to predict the mitigation potential of on-farm GHG emissions for individual farms or farm co-ops (Bergtold et al., 2019; Blanco-Canqui et al., 2015; Bossio et al., 2020; Chahal et al., 2020; Fargione et al., 2018; Griscom et al., 2017).

EC ERF can estimate total annual carbon budgets by accounting for total CO_2 fluxes of the landscape, including nighttime respiration, in contrast to RS models which only predicted carbon fluxes during daytime. While similar results could be achieved by placing shorter (3 m) EC towers in individual fields, the cost of doing so would be substantially larger compared to a single tower. Furthermore, tower maintenance in agricultural systems can be problematic, particularly for fields of intensive agricultural management, which may require moving the towers multiple times during the year. A taller (30 m) tower combined with the ERF approach could decrease maintenance costs as well as data gaps due to instrumentation relocation. Similarly, MQY could be quantified manually via instruments that measure photosynthetic parameters (i.e., Li-6800, Licor Inc.), however the spatial scales of such measurements are substantially lower compared to what EC towers can achieve, or would require intensive labor costs to cover larger areas within a field.

We found that ERF NEP projections were close to annual NEP estimates of common vegetation types. Similarly, hourly and monthly NEE timeseries correlated well with the NEE time series from the US-DFK tower, that was located close by, thus improving the cost efficiency of EC towers by extending their information collection reach. For example, projections of annual NEP (Figure 5) for the IWG field at the USDFRC farm were around 400–500 g C m^{-2}, which corresponded well with estimates of one year old IWG stands in Kansas and Minnesota

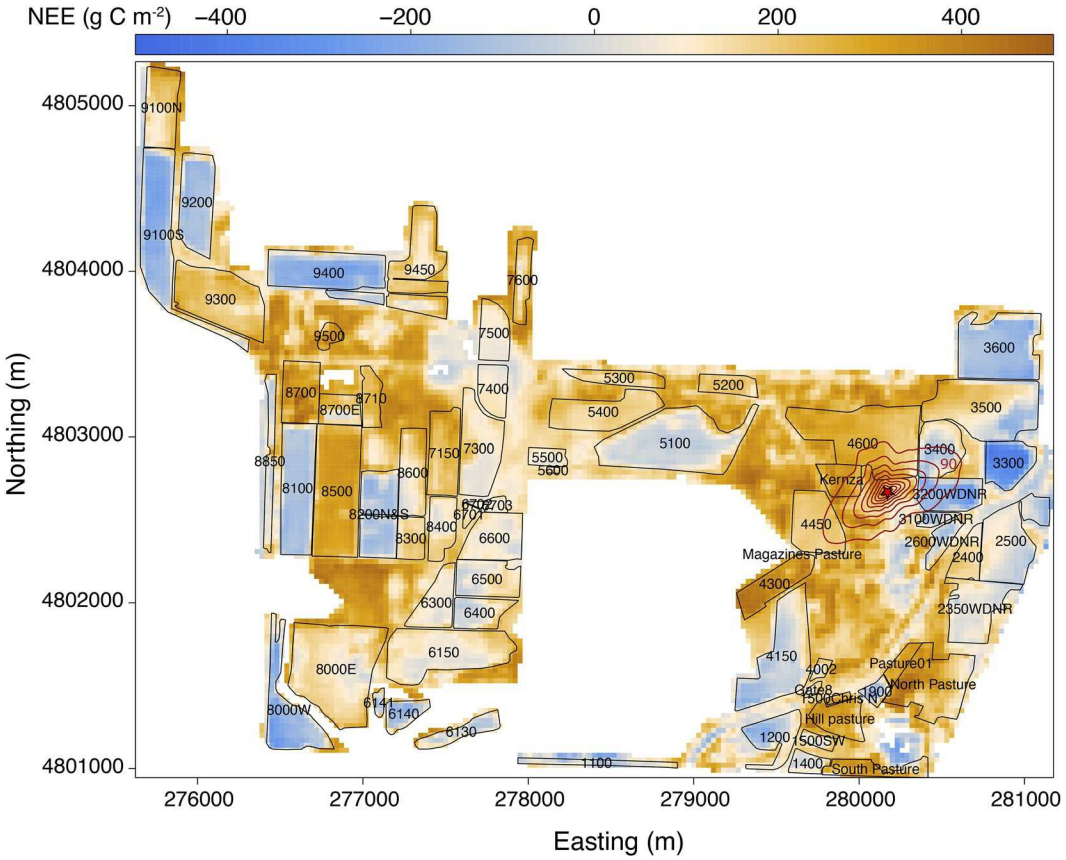

Figure 5. Annual farm net ecosystem exchange of carbon (NEE, in g C m^{-2}) calculated from daytime and nighttime eddy covariance (EC) data and hourly environmental response function (ERF) results. Here negative NEE (blue) indicates carbon loss from the system, whereas positive values (brown) indicate carbon uptake. Text and numbers represent farm crop field identifiers. The red star indicates the location of the EC tower US-DFC. Dark red contour lines represent the footprint climatology plotted with 10 percentile intervals; the outermost contours show the 90th percentile and the innermost shows the tenth percentile.

(Oliveira et al., 2018), as well as with estimates from an EC tower (US-DFK) located within the footprint of the tower described here (US-DFC) (Wiesner et al., 2022). Winter wheat annual NEP budgets were also close to what other studies found in temperate regions, amounting to ~200 g C m^{-2} (Schmidt et al., 2012). Additionally, while studies using semi-empirical light use efficiency models often assume similar MQY values for corn (Madugundu et al., 2016; Marshall et al., 2018), we found that ERF could distinguish between corn silage and corn grain fields, suggesting differences in MQY for both crop types. This substantially improved the harvest biomass prediction of both crops, but especially of corn silage, which had a lower MQY compared to corn grain.

Our results indicate that the direct MQY estimation from ERF timeseries using all datapoints resulted in an over-prediction of yields ($Harvest_{Lit}$ and $Harvest_{Field}$) for alfalfa, soybeans, and wheat fields by 20%–50% (Figure S1 in Supporting Information S1), while $RS_{ERF,gs}$ resulted in a slight underprediction of yields, based on the inclusion of heterotrophic nighttime respiration. A likely cause for the lower predictive power of $RS_{ERF,all}$ are low activity times during fallow, winter, and harvest as well as other management operations for crops compared to perennial vegetation. Such agricultural management can disrupt plant photosynthesis and lead to greater heterotrophic (i.e., decomposition of crop residues) and autotrophic respiration (i.e., regrowth following harvest). This was likely not accurately captured by RS inputs (i.e., EVI and LST), due to the lower temporal resolution of Landsat data (16 days) compared to management activity. These variations in respiration are difficult to incorporate when calculating light use efficiency parameters from annual half-hourly/hourly NEE time series. Furthermore, daytime ERF respiration calculated using REddyProc was lower compared to RS R_{eco} (by ~50%), suggesting limitations associated with the partitioning of spatiotemporal NEE time series into GPP and R_{eco}, when meteorological data (i.e., VPD, T_{air} and radiation) are only available from one location within the farm setting (US-DFC

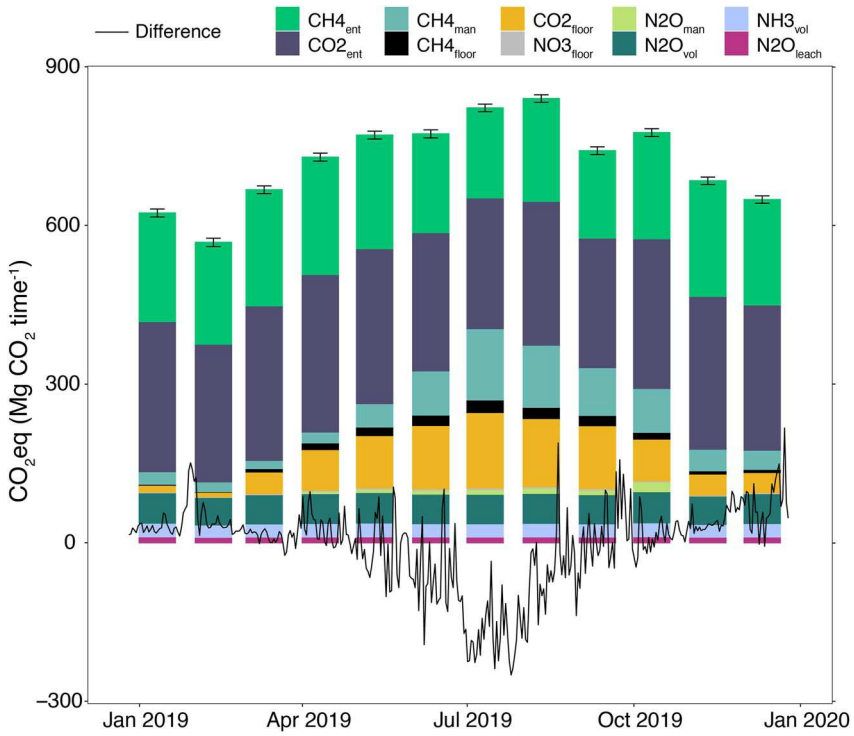

Figure 6. Barn and field emissions by month converted to CO_{2eq} for direct comparisons, where $CH_{4,ent}$ is enteric fermentation to methane, $CO_{2,ent}$ enteric CO_2, $CH_{4,man}$ is manure CH_4 emissions, $CH_{4,floor}$, $CO_{2,floor}$, and $NH_{3,floor}$ are barn floor CH_4, CO_2 and NH_3 emissions, respectively, N_2O_{man} is manure N_2O emissions, N_2O_{vol} and $NH_{3,vol}$ are indirect volatile N_2O and NH_3 emissions and N_2O_{leach} are N_2O emissions from leaching of the manure pit. Error bars indicate average daily uncertainty in emission estimates. The black line depicts the difference in daily sums of ERF NEP of CO_2 (from daytime and nighttime data) and barnyard and field emissions, where negative values indicate greater mitigation.

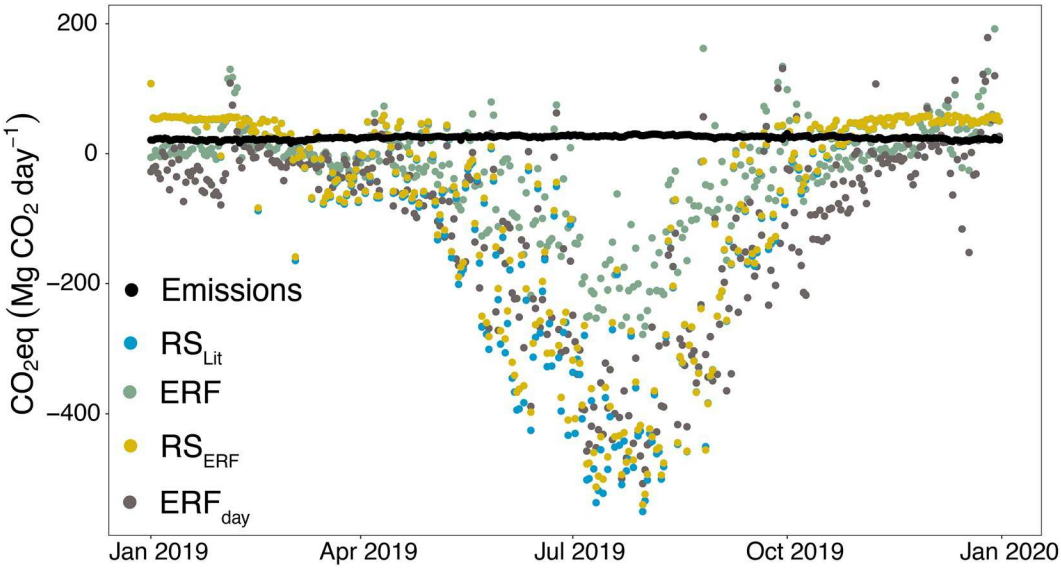

Figure 7. Daily time series of total barnyard emissions in CO_{2eq} versus daily time series of daytime and nighttime eddy covariance net ecosystem productivity (NEP) sums using the environmental response functions approach (ERF) and daytime eddy covariance NEP sums (ERF_{day}), as well as daily remote sensing NEP results calculated using maximum quantum yield values from literature data (RS_{Lit}) and MQY results from growing season daytime date (RS_{ERF}).

tower). Nighttime EC data are subject to higher uncertainty, due to the application of friction velocity (u*) or other filters to remove observations that show low coupling of the land with the atmosphere and high atmospheric stability (Novick et al., 2004; Pastorello et al., 2020).

Nevertheless, for carbon trading programs, NEE time series would be of higher interest because they quantify changes in carbon stocks (Paustian et al., 2019). Best results were obtained using daytime ERF NEP data points from the growing season, which resulted in an improved fit when comparing to $Harvest_{Lit}$ and $Harvest_{Field}$, in contrast to both ERF time series and RS_{Lit}. Correlations between RS_{Lit} and ERF were highest during the growing season (May-October). This was a function of the structure of RS models which predicted more respiration during the shoulder season, as minimum temperature was set to −1°C following Zhang et al. (2017), thus assuming no photosynthetic activity when temperatures were low. Nevertheless, pastures and other perennial vegetation types can remain green and photosynthetically active during winter, and even under the snow (Skinner, 2007), which was better captured by EC ERF. However, while ERF_{day} data improved the prediction of biomass accumulation, total ERF NEE results captured the full carbon balance, including nighttime respiration. ERF_{day} and RS models correlated well as RS models included daylight hours only (i.e., PAR, EVI and LST); Landsat and MODIS sensors pass the USDFRC location during the hours of 11 a.m. and 2 p.m. local time (Barnes et al., 2014; Pahlevan et al., 2014). This suggests that daytime respiration was predicted well using RS models, while nighttime respiration was unaccounted for.

We found further limitations in our predictions when extracting MQY from mixed forests at the farm, which was related to their patchiness and the assumption that forest productivity would be similar among species within the same location. While tree species at the farm were composed of more broadleaf species than coniferous, we would expect differences in MQY based on variations in tree physiology (Li et al., 2018; Wong et al., 2019). Because we did not have information on species composition and their spatial locations, we used only one shapefile polygon for the forest, shrub, and grass locations each to extract NEE/NEP from ERF and RS models. However, as shown in Figure 5, forest productivity varied by location (i.e., to the north and west of field 4,600). This likely led to an underprediction of CO_2 uptake of forests using ERF_{MQY}. To better account for these physiological variations spatial information on species composition would be needed to extract times series and to calculate MQY by plant functional type.

5. Conclusions

We found that updating MQY values in RS models using EC-ERF significantly improved the prediction of crop yields at the USDFRC dairy farm. The range of data variability decreased and the overall fit of harvest predictions and measured yields improved by ∼10%. Our evaluation of strategies found that using spatiotemporal EC-ERF data with commonly used RS approaches provides a viable economic pathway by reducing the number of towers needed to quantify land-atmosphere interactions of mixed ecosystems for real-time assessment of NCS.

Using this approach, for 2019, we found that the USDFRC farm was a net zero dairy farm when emissions, but not farm exports, were accounted for. Natural perennial vegetation types, while only accounting for 40% of the landscape, mitigated over 60% of all barnyard and field emissions. However, with the inclusion of milk and harvest exports, the dairy farm exceeded net zero by 2.6 Gg of CO_2, indicating the negative implications of harvest exports, specifically for soybeans, which are grown, in part, for crop rotation benefits. This was further exacerbated by annual carbon balances of soybean fields, which were all close to 0 g C yr^{-1}, likely due to the short growing season and because soybeans are often planted following corn, further lowering carbon inputs from residues. Interannual time of lowest mitigation potentials were found for manure spreading and harvest seasons, despite higher monthly emissions during the summer months.

Our results suggest that integrated crop-livestock systems that grow most cattle feed on farm can reach net zero when ∼1/3 of the landscape is perennial vegetation like forests, shrublands, grasslands and pastures, as well as when nutrient applications are managed according to crop needs following precision agriculture guidelines, rather than more common spring and fall application periods. The implementation of perennial vegetation such as forest and grasslands in dairy systems could be used as NCS to reduce and/or mitigate on farm GHG emissions, in addition to providing an array of other important ecosystem services.

Conflict of Interest

The authors declare no conflicts of interest relevant to this study.

Data Availability Statement

The RS data from Landsat and MODIS used for gross primary, ecosystem respiration and ERF calculations in the study are available at https://www.usgs.gov/. EC data can be found at https://ameriflux.lbl.gov/sites/siteinfo/US-DFC. The farm herd, feed, nutrient, manure and fertilizer, harvest and milk data, as well as information on ERF machine learning can be found at https://zenodo.org/record/6772181. The ERF code used for the EC ERF NEE maps is preserved at https://github.com/NEONScience/NEON-FIU-algorithm, available via user agreement license.

Acknowledgments
SW and PS acknowledge funding from the Wisconsin Dairy Innovation Hub. All authors would like to thank Jonathan Thom for help during instrumentation and data upkeep. Additionally, all authors would like to thank the USDFRC technical support and farm management team. The authors would like to acknowledge and honor that both the University of Wisconsin–Madison, as well as the US Dairy Forage Research Center farm at Prairie du Sac, where this research took place, occupy ancestral Ho-Chunk land, which the Ho-Chunk Nation was forced to cede in 1832. As researchers we value and respect the sovereignty of the Ho-Chunk Nation, along with the 11 other First Nations of Wisconsin. The Nation's continued land stewardship and resource management is a powerful example of how natural climate solutions, through a close connection to the land, can help maintain societal, economic, and ecological sustainability. The National Ecological Observatory Network is a program sponsored by the National Science Foundation and operated under cooperative agreement by Battelle. This material is based in part upon work supported by the National Science Foundation through the NEON Program. This material is based upon work supported by the National Science Foundation under Award Numbers DBI-0735191, DBI-1265383, and DBI-1743442. URL: www.cyverse.org.

References

Agostini, F., Gregory, A. S., & Richter, G. M. (2015). Carbon sequestration by perennial energy crops: Is the Jury still out? *BioEnergy Research*, *8*(3), 1057–1080. https://doi.org/10.1007/s12155-014-9571-0

Anderson, C. M., DeFries, R. S., Litterman, R., Matson, P. A., Nepstad, D. C., Pacala, S., et al. (2019). Natural climate solutions are not enough. *Science*, *363*(6430), 933–934. https://doi.org/10.1126/science.aaw2741

Anderson, M., Gao, F., Knipper, K., Hain, C., Dulaney, W., Baldocchi, D., et al. (2018). Field-scale Assessment of land and water use change over the California delta using remote sensing. *Remote Sensing*, *10*(6), 889. https://doi.org/10.3390/rs10060889

Baek, J., Alhindi, T. J., Jeong, Y. S., Jeong, M. K., Seo, S., Kang, J., et al. (2021). Real-time fire detection system based on dynamic time warping of multichannel sensor networks. *Fire Safety Journal*, *123*, 103364. https://doi.org/10.1016/j.firesaf.2021.103364

Barnes, B. B., Hu, C., Holekamp, K. L., Blonski, S., Spiering, B. A., Palandro, D., & Lapointe, B. (2014). Use of Landsat data to track historical water quality changes in Florida Keys marine environments. *Remote Sensing of Environment*, *140*, 485–496. https://doi.org/10.1016/j.rse.2013.09.020

Bellamy, R., & Osaka, S. (2020). Unnatural climate solutions? *Nature Climate Change*, *10*(2), 98–99. https://doi.org/10.1038/s41558-019-0661-z

Bellman, R., & Kalaba, R. (1959). On adaptive control processes. *IRE Transactions on Automatic Control*, *4*(2), 1–9. https://doi.org/10.1109/TAC.1959.1104847

Bergtold, J. S., Ramsey, S., Maddy, L., & Williams, J. R. (2019). A review of economic considerations for cover crops as a conservation practice. *Renewable Agriculture and Food Systems*, *34*(1), 62–76. https://doi.org/10.1017/s1742170517000278

Beukes, P. C., Gregorini, P., Romera, A. J., Levy, G., & Waghorn, G. C. (2010). Improving production efficiency as a strategy to mitigate greenhouse gas emissions on pastoral dairy farms in New Zealand. *Agriculture, Ecosystems & Environment*, *136*(3–4), 358–365. https://doi.org/10.1016/j.agee.2009.08.008

Blanco-Canqui, H., Shaver, T. M., Lindquist, J. L., Shapiro, C. A., Elmore, R. W., Francis, C. A., & Hergert, G. W. (2015). Cover crops and ecosystem services: Insights from studies in temperate soils. *Agronomy Journal*, *107*(6), 2449–2474. https://doi.org/10.2134/agronj15.0086

Bloch-Johnson, J., Rugenstein, M., Stolpe, M. B., Rohrschneider, T., Zheng, Y., & Gregory, J. M. (2021). Climate sensitivity increases under higher CO_2 levels due to feedback temperature dependence. *Geophysical Research Letters*, *48*(4). https://doi.org/10.1029/2020gl089074

Bolinder, M. A., Janzen, H. H., Gregorich, E. G., Angers, D. A., & VandenBygaart, A. J. (2007). An approach for estimating net primary productivity and annual carbon inputs to soil for common agricultural crops in Canada. *Agriculture, Ecosystems & Environment*, *118*(1–4), 29–42. https://doi.org/10.1016/j.agee.2006.05.013

Bossio, D. A., Cook-Patton, S. C., Ellis, P. W., Fargione, J., Sanderman, J., Smith, P., et al. (2020). The role of soil carbon in natural climate solutions. *Nature Sustainability*, *3*(5), 391–398. https://doi.org/10.1038/s41893-020-0491-z

Bowen, F., & Wittneben, B. (2011). Carbon accounting: Negotiating accuracy, consistency and certainty across organisational fields. *Accounting, Auditing & Accountability Journal*, *24*(8), 1022–1036. https://doi.org/10.1108/09513571111184742

Brock, F. V. (1986). A nonlinear filter to remove impulse noise from meteorological data. *Journal of Atmospheric and Oceanic Technology*, *3*(1), 51–58. https://doi.org/10.1175/1520-0426(1986)003<0051:anftri>2.0.co;2

Butterworth, B. J., Desai, A. R., Townsend, P. A., Petty, G. W., Andresen, C. G., Bertram, E. T. H., et al. (2021). Connecting land–atmosphere interactions to surface heterogeneity in CHEESEHEAD19. *Bulletin of the American Meteorological Society*, *102*(2), E421–E445. https://doi.org/10.1175/BAMS-D-19-0346.1

Chahal, I., Vyn, R. J., Mayers, D., & Eerd, L. L. V. (2020). Cumulative impact of cover crops on soil carbon sequestration and profitability in a temperate humid climate. *Scientific Reports*, *10*(1), 13381. https://doi.org/10.1038/s41598-020-70224-6

Chen, B., Ge, Q., Fu, D., Yu, G., Sun, X., Wang, S., & Wang, H. (2010). A data-model fusion approach for upscaling gross ecosystem productivity to the landscape scale based on remote sensing and flux footprint modelling. *Biogeosciences*, *7*(9), 2943–2958. https://doi.org/10.5194/bg-7-2943-2010

Chu, H., Luo, X., Ouyang, Z., Chan, W. S., Dengel, S., Biraud, S. C., et al. (2021). Representativeness of eddy-covariance flux footprints for areas surrounding AmeriFlux sites. *Agricultural and Forest Meteorology*, *301*, 108350. https://doi.org/10.1016/j.agrformet.2021.108350

Colomb, V., Touchemoulin, O., Bockel, L., Chotte, J.-L., Martin, S., Tinlot, M., & Bernoux, M. (2013). Selection of appropriate calculators for landscape-scale greenhouse gas assessment for agriculture and forestry. *Environmental Research Letters*, *8*(1), 015029. https://doi.org/10.1088/1748-9326/8/1/015029

Crous, K. Y. (2019). Plant responses to climate warming: Physiological adjustments and implications for plant functioning in a future, warmer world. *American Journal of Botany*, *106*(8), 1049–1051. https://doi.org/10.1002/ajb2.1329

de Oliveira, G., Brunsell, N. A., Sutherlin, C. E., Crews, T. E., & DeHaan, L. R. (2018). Energy, water and carbon exchange over a perennial Kernza wheatgrass crop. *Agricultural and Forest Meteorology*, *249*, 120–137. https://doi.org/10.1016/j.agrformet.2017.11.022

Didan, K. (2015). MOD13Q1 MODIS/Terra vegetation indices 16-Day L3 Global 250m SIN Grid V006. https://doi.org/10.5067/MODIS/MOD13Q1.006

Dusenge, M. E., Duarte, A. G., & Way, D. A. (2019). Plant carbon metabolism and climate change: Elevated CO_2 and temperature impacts on photosynthesis, photorespiration and respiration. *New Phytologist*, *221*(1), 32–49. https://doi.org/10.1111/nph.15283

Fargione, J. E., Bassett, S., Boucher, T., Bridgham, S. D., Conant, R. T., Cook-Patton, S. C., et al. (2018). Natural climate solutions for the United States. *Science Advances*, *4*(11), eaat1869. https://doi.org/10.1126/sciadv.aat1869

Fleischman, F., Basant, S., Chhatre, A., Coleman, E. A., Fischer, H. W., Gupta, D., et al. (2020). Pitfalls of tree planting show why we need people-centered natural climate solutions. *BioScience*. https://doi.org/10.1093/biosci/biaa094

Foken, T. (2008). The energy balance closure problem: An overview. *Ecological Applications*, *18*(6), 1351–1367. https://doi.org/10.1890/06-0922.1

Foken, T., & Wichura, B. (1996). Tools for quality assessment of surface-based flux measurements. *Agricultural and Forest Meteorology*, *78*(1–2), 83–105. https://doi.org/10.1016/0168-1923(95)02248-1

Fu, D., Chen, B., Zhang, H., Wang, J., Black, T. A., Amiro, B. D., et al. (2014). Estimating landscape net ecosystem exchange at high spatial–temporal resolution based on Landsat data, an improved upscaling model framework, and eddy covariance flux measurements. *Remote Sensing of Environment*, *141*, 90–104. https://doi.org/10.1016/j.rse.2013.10.029

Fuglestvedt, J., Rogelj, J., Millar, R. J., Allen, M., Boucher, O., Cain, M., et al. (2018). Implications of possible interpretations of greenhouse gas balance in the Paris Agreement. *Philosophical Transactions of the Royal Society A: Mathematical, Physical & Engineering Sciences*, *376*(2119), 20160445. https://doi.org/10.1098/rsta.2016.0445

Gao, Y., Yu, G., Li, S., Yan, H., Zhu, X., Wang, Q., et al. (2015). A remote sensing model to estimate ecosystem respiration in Northern China and the Tibetan Plateau. *Ecological Modelling*, *304*, 34–43. https://doi.org/10.1016/j.ecolmodel.2015.03.001

Giorgino, T. (2009). Computing and visualizing dynamic time warping alignments in R: The dtw package. *Journal of Statistical Software*, *31*(7). https://doi.org/10.18637/jss.v031.i07

Graves, R. A., Haugo, R. D., Holz, A., Nielsen-Pincus, M., Jones, A., Kellogg, B., et al. (2020). Potential greenhouse gas reductions from natural climate solutions in Oregon, USA. *PLoS One*, *15*(4), e0230424. https://doi.org/10.1371/journal.pone.0230424

Griscom, B. W., Adams, J., Ellis, P. W., Houghton, R. A., Lomax, G., Miteva, D. A., et al. (2017). Natural climate solutions. *Proceedings of the National Academy of Sciences*, *114*(44), 11645–11650. https://doi.org/10.1073/pnas.1710465114

Hannun, R. A., Wolfe, G. M., Kawa, S. R., Hanisco, T. F., Newman, P. A., Alfieri, J. G., et al. (2020). Spatial heterogeneity in CO_2, CH_4, and energy fluxes: Insights from airborne eddy covariance measurements over the Mid-Atlantic region. *Environmental Research Letters*, *15*(3), 035008. https://doi.org/10.1088/1748-9326/ab7391

Helbig, M., Gerken, T., Beamesderfer, E. R., Baldocchi, D. D., Banerjee, T., Biraud, S. C., et al. (2021). Integrating continuous atmospheric boundary layer and tower-based flux measurements to advance understanding of land-atmosphere interactions. *Agricultural and Forest Meteorology*, *307*, 108509. https://doi.org/10.1016/j.agrformet.2021.108509

Hemes, K. S., Runkle, B. R. K., Novick, K. A., Baldocchi, D. D., & Field, C. B. (2021). An ecosystem-scale flux measurement strategy to assess natural climate solutions. *Environmental Science and Technology*, *55*(6), 3494–3504. https://doi.org/10.1021/acs.est.0c06421

Hickey, L. T., Hafeez, A. N., Robinson, H., Jackson, S. A., Leal-Bertioli, S. C. M., Tester, M., et al. (2019). Breeding crops to feed 10 billion. *Nature Biotechnology*, *37*(7), 744–754. https://doi.org/10.1038/s41587-019-0152-9

Hijmans, R. J. (2021). raster: Geographic data analysis and modeling. R package version 3.4-13. Retrieved from https://CRAN.R-project.org/package=raster

Huang, X., Xiao, J., Wang, X., & Ma, M. (2021). Improving the global MODIS GPP model by optimizing parameters with FLUXNET data. *Agricultural and Forest Meteorology*, *300*, 108314. https://doi.org/10.1016/j.agrformet.2020.108314

IPCC. (2006). 2006 IPCC guidelines for national greenhouse gas inventories. Prepared by the National Greenhouse Gas Inventories Programme (Intergovernmental Panel on Climate Change).

Jayasundara, S., Worden, D., Weersink, A., Wright, T., VanderZaag, A., Gordon, R., & Wagner-Riddle, C. (2019). Improving farm profitability also reduces the carbon footprint of milk production in intensive dairy production systems. *Journal of Cleaner Production*, *229*, 1018–1028. https://doi.org/10.1016/j.jclepro.2019.04.013

Jiang, S., Zhao, L., Liang, C., Cui, N., Gong, D., Wang, Y., et al. (2021). Comparison of satellite-based models for estimating gross primary productivity in agroecosystems. *Agricultural and Forest Meteorology*, *297*, 108253. https://doi.org/10.1016/j.agrformet.2020.108253

Joiner, J., Yoshida, Y., Zhang, Y., Duveiller, G., Jung, M., Lyapustin, A., et al. (2018). Estimation of terrestrial global gross primary production (GPP) with satellite data-driven models and eddy covariance flux data. *Remote Sensing*, *10*(9), 1346. https://doi.org/10.3390/rs10091346

Joy, S. L., & Chávez, J. L. (2021). Correction of eddy covariance based crop ET considering the heat flux source area. *Atmosphere*, *12*(2), 281. https://doi.org/10.3390/atmos12020281

Kelley, D., & Richards, C. (2021). oce: Analysis of Oceanographic Data. R package version 1.4-0. Retrieved from https://CRAN.R-project.org/package=oce

Kelley, D. E. (2018). The oce package. *Oceanographic Analysis with R*, 91–101. https://doi.org/10.1007/978-1-4939-8844-0_3

Kljun, N., Calanca, P., Rotach, M. W., & Schmid, H. P. (2004). A simple parameterisation for flux footprint predictions. *Boundary-Layer Meteorology*, *112*(3), 503–523. https://doi.org/10.1023/b:boun.0000030653.71031.96

Knauer, J., El-Madany, T. S., Zaehle, S., & Migliavacca, M. (2018). Bigleaf—An R package for the calculation of physical and physiological ecosystem properties from eddy covariance data. *PLoS One*, *13*(8), e0201114. https://doi.org/10.1371/journal.pone.0201114

Krause, P., Boyle, D. P., & Bäse, F. (2005). Comparison of different efficiency criteria for hydrological model assessment. *Advances in Geosciences*, *5*, 89–97. https://doi.org/10.5194/adgeo-5-89-2005

Leahy, S., Clark, H., & Reisinger, A. (2020). Challenges and prospects for agricultural greenhouse gas mitigation pathways consistent with the Paris agreement. *Frontiers in Sustainable Food Systems*, *4*, 69. https://doi.org/10.3389/fsufs.2020.00069

Li, Y., He, N., Hou, J., Xu, L., Liu, C., Zhang, J., et al. (2018). Factors influencing leaf chlorophyll content in natural forests at the Biome scale. *Frontiers in Ecology and Evolution*, *6*, 64. https://doi.org/10.3389/fevo.2018.00064

Little, S., Benchaar, C., Janzen, H., Kröbel, R., McGeough, E., & Beauchemin, K. (2017). Demonstrating the effect of forage source on the carbon footprint of a Canadian dairy farm using whole-systems analysis and the Holos model: Alfalfa silage vs. Corn silage. *Climate*, *5*(4), 87. https://doi.org/10.3390/cli5040087

Lloyd, J., & Taylor, J. A. (1994). On the temperature dependence of soil respiration. *Functional Ecology*, *8*(3), 315. https://doi.org/10.2307/2389824

Lubbe, F. C., Klimešová, J., & Henry, H. A. L. (2021). Winter belowground: Changing winters and the perennating organs of herbaceous plants. *Functional Ecology*, *35*(8), 1627–1639. https://doi.org/10.1111/1365-2435.13858

Madugundu, R., Al-Gaadi, K. A., Tola, E., Kayad, A. G., & Jha, C. S. (2016). Estimation of gross primary production of irrigated maize using Landsat-8 imagery and Eddy Covariance data. *Saudi Journal of Biological Sciences*, *24*(2), 410–420. https://doi.org/10.1016/j.sjbs.2016.10.003

Marshall, M., Tu, K., & Brown, J. (2018). Optimizing a remote sensing production efficiency model for macro-scale GPP and yield estimation in agroecosystems. *Remote Sensing of Environment*, *217*, 258–271. https://doi.org/10.1016/j.rse.2018.08.001

McCallum, I., Wagner, W., Schmullius, C., Shvidenko, A., Obersteiner, M., Fritz, S., & Nilsson, S. (2009). Satellite-based terrestrial production efficiency modeling. *Carbon Balance and Management*, *4*(1), 8. https://doi.org/10.1186/1750-0680-4-8

Meena, R. K., Reddy, K. S., Gautam, R., Maddela, S., Reddy, A. R., & Gudipalli, P. (2021). Improved photosynthetic characteristics correlated with enhanced biomass in a heterotic F1 hybrid of maize (Zea mays L.). *Photosynthesis Research*, *147*(3), 253–267. https://doi.org/10.1007/s11120-021-00822-6

Metzger, J. P., Villarreal-Rosas, J., Suárez-Castro, A. F., López-Cubillos, S., González-Chaves, A., Runting, R. K., et al. (2021). Considering landscape-level processes in ecosystem service assessments. *The Science of the Total Environment*, *796*, 149028. https://doi.org/10.1016/j.scitotenv.2021.149028

Metzger, S. (2018). Surface-atmosphere exchange in a box: Making the control volume a suitable representation for in-situ observations. *Agricultural and Forest Meteorology*, *255*, 68–80. https://doi.org/10.1016/j.agrformet.2017.08.037

Metzger, S., Junkermann, W., Mauder, M., Butterbach-Bahl, K., Widemann, B. T. y., Neidl, F., et al. (2013). Spatially explicit regionalization of airborne flux measurements using environmental response functions. *Biogeosciences*, *10*(4), 2193–2217. https://doi.org/10.5194/bg-10-2193-2013

Novick, K. A., Metzger, S., Anderegg, W. R., Barnes, M., Cala, D. S., Guan, K., et al. (2022). Informing nature-based climate solutions for the United States with the best-available science. *Global Change Biology*, *28*(12), 3778–3794. https://doi.org/10.1111/gcb.16156

Novick, K. A., Stoy, P. C., Katul, G. G., Ellsworth, D. S., Siqueira, M. B. S., Juang, J., & Oren, R. (2004). Carbon dioxide and water vapor exchange in a warm temperate grassland. *Oecologia*, *138*(2), 259–274. https://doi.org/10.1007/s00442-003-1388-z

Ogutu, B. O., Dash, J., & Dawson, T. P. (2013). Developing a diagnostic model for estimating terrestrial vegetation gross primary productivity using the photosynthetic quantum yield and Earth observation data. *Global Change Biology*, *19*(9), 2878–2892. https://doi.org/10.1111/gcb.12261

Olander, L., Wollenberg, E., Tubiello, F., & Herold, M. (2013). Advancing agricultural greenhouse gas quantification*. *Environmental Research Letters*, *8*(1), 011002. https://doi.org/10.1088/1748-9326/8/1/011002

Olmedo, G., FedericoOrtega-Farías, S., de la Fuente-Sáiz, D., Fonseca-Luego, D., & Fuentes-Peñailillo, F. (2016). Water: Tools and functions to estimate actual evapotranspiration using land surface energy balance models in R. *The R Journal*, *8*(2), 352. https://doi.org/10.32614/rj-2016-051

Pahlevan, N., Lee, Z., Wei, J., Schaaf, C. B., Schott, J. R., & Berk, A. (2014). On-orbit radiometric characterization of OLI (Landsat-8) for applications in aquatic remote sensing. *Remote Sensing of Environment*, *154*, 272–284. https://doi.org/10.1016/j.rse.2014.08.001

Paitan, C. P., & Verburg, P. H. (2019). Methods to assess the impacts and indirect land use change caused by telecoupled agricultural supply chains: A review. *Sustainability*, *11*(4), 1162. https://doi.org/10.3390/su11041162

Pastorello, G., Trotta, C., Canfora, E., Chu, H., Christianson, D., Cheah, Y.-W., et al. (2020). The FLUXNET2015 dataset and the ONEFlux processing pipeline for eddy covariance data. *Scientific Data*, *7*(1), 225. https://doi.org/10.1038/s41597-020-0534-3

Paustian, K., Collier, S., Baldock, J., Burgess, R., Creque, J., DeLonge, M., et al. (2019). Quantifying carbon for agricultural soil management: From the current status toward a global soil information system. *Carbon Management*, *10*(6), 1–21. https://doi.org/10.1080/17583004.2019.1633231

Pique, G., Fieuzal, R., Bitar, A. A., Veloso, A., Tallec, T., Brut, A., et al. (2020). Estimation of daily CO_2 fluxes and of the components of the carbon budget for winter wheat by the assimilation of Sentinel 2-like remote sensing data into a crop model. *Geoderma*, *376*, 114428. https://doi.org/10.1016/j.geoderma.2020.114428

Prince, S. D., Haskett, J., Steininger, M., Strand, H., & Wright, R. (2001). Net primary production of US Midwest croplands from agricultural harvest yield data. *Ecological Applications*, *11*(4), 1194–1205. https://doi.org/10.1890/1051-0761(2001)011[1194:nppous]2.0.co;2

Rafi, Z., Merlin, O., Dantec, V. L., Khabba, S., Er-Raki, S., & Mordelet, P. (2020). Advances in Smart technologies applications and case studies, selected papers from the first international conference on smart information and communication technologies, SmartICT 2019, September 26-28, 2019, Saidia, Morocco. *Lecture Notes in Electrical Engineering*, 431–439. https://doi.org/10.1007/978-3-030-53187-4_47

Ribeiro-Filho, H. M. N., Civiero, M., & Kebreab, E. (2020). Potential to reduce greenhouse gas emissions through different dairy cattle systems in subtropical regions. *PLoS One*, *15*(6), e0234687. https://doi.org/10.1371/journal.pone.0234687

Rosenstock, T. S., Rufino, M. C., Butterbach-Bahl, K., & Wollenberg, E. (2013). Toward a protocol for quantifying the greenhouse gas balance and identifying mitigation options in smallholder farming systems. *Environmental Research Letters*, *8*(2), 021003. https://doi.org/10.1088/1748-9326/8/2/021003

Running, S. W., Nemani, R., Glassy, J. M., & Thornton, P. E. (1999). *MODIS daily photosynthesis (PSN) and annual net primary production (NPP) product (MOD17) Algorithm Theoretical Basis Document*. NASA. Retrieved from https://modis.gsfc.nasa.gov/data/atbd/atbd_mod16.pdf

Running, S. W., & Zhao, M. (2015). User's guide daily GPP and annual NPP (MOD17A2/A3) products NASA Earth observing system MODIS land algorithm. Retrieved from https://www.ntsg.umt.edu/files/modis/MOD17UsersGuide2015_v3.pdf

Saggar, S., Giltrap, D. L., Davison, R., Gibson, R., de Klein, C. A. M., Rollo, M., et al. (2015). Estimating direct N_2O emissions from sheep, beef, and deer grazed pastures in New Zealand hill country: Accounting for the effect of land slope on the N_2O emission factors from urine and dung. *Agriculture, Ecosystems & Environment*, *205*, 70–78. https://doi.org/10.1016/j.agee.2015.03.005

Schmidt, M., Reichenau, T. G., Fiener, P., & Schneider, K. (2012). The carbon budget of a winter wheat field: An eddy covariance analysis of seasonal and inter-annual variability. *Agricultural and Forest Meteorology*, *165*, 114–126. https://doi.org/10.1016/j.agrformet.2012.05.012

Schotanus, P., Nieuwstadt, F. T. M., & Bruin, H. A. R. D. (1983). Temperature measurement with a sonic anemometer and its application to heat and moisture fluxes. *Boundary-Layer Meteorology*, *26*(1), 81–93. https://doi.org/10.1007/bf00164332

Schwarze, R., Niles, J. O., & Olander, J. (2002). Understanding and managing leakage in forest-based greenhouse-gas-mitigation projects. *Philosophical Transactions of the Royal Society of London, Series A: Mathematical, Physical and Engineering Sciences*, *360*(1797), 1685–1703. https://doi.org/10.1098/rsta.2002.1040

Shao, G., Li, Z., Ning, T., & Zheng, Y. (2013). Responses of photosynthesis, chlorophyll fluorescence, and grain yield of maize to controlled-release urea and irrigation after anthesis. *Journal of Plant Nutrition and Soil Science*, *176*(4), 595–602. https://doi.org/10.1002/jpln.201100185

Shine, K. P., Fuglestvedt, J. S., Hailemariam, K., & Stuber, N. (2005). Alternatives to the global warming potential for comparing climate impacts of emissions of greenhouse gases. *Climatic Change*, *68*(3), 281–302. https://doi.org/10.1007/s10584-005-1146-9

Sishodia, R. P., Ray, R. L., & Singh, S. K. (2020). Applications of remote sensing in precision agriculture: A review. *Remote Sensing*, *12*(19), 3136. https://doi.org/10.3390/rs12193136

Skinner, H. (2007). Winter carbon dioxide fluxes in humid-temperate pastures. *Agricultural and Forest Meteorology*, *144*(1–2), 32–43. https://doi.org/10.1016/j.agrformet.2007.01.010

Sleeter, B. M., Liu, J., Daniel, C., Rayfield, B., Sherba, J., Hawbaker, T. J., et al. (2018). Effects of contemporary land-use and land-cover change on the carbon balance of terrestrial ecosystems in the United States. *Environmental Research Letters*, *13*(4), 045006. https://doi.org/10.1088/1748-9326/aab540

Smith, P., Soussana, J., Angers, D., Schipper, L., Chenu, C., Rasse, D. P., et al. (2019). How to measure, report and verify soil carbon change to realize the potential of soil carbon sequestration for atmospheric greenhouse gas removal. *Global Change Biology*, *26*(1), 219–241. https://doi.org/10.1111/gcb.14815

Sobrino, J. A., Jiménez-Muñoz, J. C., & Paolini, L. (2004). Land surface temperature retrieval from LANDSAT TM 5. *Remote Sensing of Environment*, *90*(4), 434–440. https://doi.org/10.1016/j.rse.2004.02.003

Starkenburg, D., Fochesatto, G. J., Cristóbal, J., Prakash, A., Gens, R., Alfieri, J. G., et al. (2015). Temperature regimes and turbulent heat fluxes across a heterogeneous canopy in an Alaskan boreal forest. *Journal of Geophysical Research: Atmospheres*, *120*(4), 1348–1360. https://doi.org/10.1002/2014jd022338

Styles, D., Gonzalez-Mejia, A., Moorby, J., Foskolos, A., & Gibbons, J. (2018). Climate mitigation by dairy intensification depends on intensive use of spared grassland. *Global Change Biology*, *24*(2), 681–693. https://doi.org/10.1111/gcb.13868

Syswerda, S. P., Basso, B., Hamilton, S. K., Tausig, J. B., & Robertson, G. P. (2012). Long-term nitrate loss along an agricultural intensity gradient in the Upper Midwest USA. *Agriculture, Ecosystems & Environment*, *149*, 10–19. https://doi.org/10.1016/j.agee.2011.12.007

Teets, A., Fraver, S., Hollinger, D. Y., Weiskittel, A. R., Seymour, R. S., & Richardson, A. D. (2018). Linking annual tree growth with eddy-flux measures of net ecosystem productivity across twenty years of observation in a mixed conifer forest. *Agricultural and Forest Meteorology*, *249*, 479–487. https://doi.org/10.1016/j.agrformet.2017.08.007

Vickers, D., & Mahrt, L. (1997). Quality control and flux sampling problems for tower and aircraft data. *Journal of Atmospheric and Oceanic Technology*, *14*(3), 512–526. https://doi.org/10.1175/1520-0426(1997)014<0512:qcafsp>2.0.co;2

Voglmeier, K., Six, J., Jocher, M., & Ammann, C. (2020). Soil greenhouse gas budget of two intensively managed grazing systems. *Agricultural and Forest Meteorology*, *287*, 107960. https://doi.org/10.1016/j.agrformet.2020.107960

Vyse, K., Pagter, M., Zuther, E., & Hincha, D. K. (2019). Deacclimation after cold acclimation—A crucial, but widely neglected part of plant winter survival. *Journal of Experimental Botany*, *70*(18), 4595–4604. https://doi.org/10.1093/jxb/erz229

Wall, A. M., Campbell, D. I., Morcom, C. P., Mudge, P. L., & Schipper, L. A. (2020). Quantifying carbon losses from periodic maize silage cropping of permanent temperate pastures. *Agriculture, Ecosystems & Environment*, *301*, 107048. https://doi.org/10.1016/j.agee.2020.107048

Wan, Z., Hook, S., & Hulley, G. (2015). MOD11A1 MODIS/Terra land surface temperature/emissivity daily L3 global 1km SIN Grid V006. https://doi.org/10.5067/MODIS/MOD11A1.006

Wang, J., Sun, R., Zhang, H., Xiao, Z., Zhu, A., Wang, M., et al. (2020a). New global MuSyQ GPPNPP remote sensing products from 1981 to 2018. *IEEE Journal of Selected Topics in Applied Earth Observations and Remote Sensing*, *14*, 5596–5612. https://doi.org/10.1109/jstars.2021.3076075

Wang, M., Sun, R., Zhu, A., & Xiao, Z. (2020b). Evaluation and comparison of light use efficiency and gross primary productivity using three different approaches. *Remote Sensing*, *12*(6), 1003. https://doi.org/10.3390/rs12061003

Waring, R. H., Landsberg, J. J., & Williams, M. (1998). Net primary production of forests: A constant fraction of gross primary production? *Tree Physiology*, *18*(2), 129–134. https://doi.org/10.1093/treephys/18.2.129

Wassmann, R., Pasco, R., Zerrudo, J., Ngo, D. M., Vo, T. B. T., & Sander, B. O. (2019). Introducing a new tool for greenhouse gas calculation tailored for cropland: Rationale, operational framework and potential application. *Carbon Management*, *10*(1), 1–14. https://doi.org/10.1080/17583004.2018.1553436

Webb, E. K., Pearman, G. I., & Leuning, R. (1980). Correction of flux measurements for density effects due to heat and water vapour transfer. *Quarterly Journal of the Royal Meteorological Society*, *106*(447), 85–100. https://doi.org/10.1002/qj.49710644707

Weiss, M., Jacob, F., & Duveiller, G. (2020). Remote sensing for agricultural applications: A meta-review. *Remote Sensing of Environment*, *236*, 111402. https://doi.org/10.1016/j.rse.2019.111402

Wiesner, S., Duff, A. J., Desai, A. R., & Panke-Buisse, K. (2020). Increasing dairy sustainability with integrated crop–livestock farming. *Sustainability*, *12*(3), 765. https://doi.org/10.3390/su12030765

Wiesner, S., Duff, A. J., Niemann, K. A. J., DesaiCrews, T. E., Picasso, V., et al. (2022). Growing season carbon dynamics differ in intermediate wheatgrass monoculture versus biculture with red clover. *Agricultural and Forest Meteorology*, *323*, 109062. https://doi.org/10.1016/j.agrformet.2022.109062

Wilczak, J. M., Oncley, S. P., & Stage, S. A. (2001). Sonic anemometer tilt correction algorithms. *Boundary-Layer Meteorology*, *99*(1), 127–150. https://doi.org/10.1023/a:1018966204465

Wong, C. Y. S., D'Odorico, P., Bhathena, Y., Arain, M. A., & Ensminger, I. (2019). Carotenoid based vegetation indices for accurate monitoring of the phenology of photosynthesis at the leaf-scale in deciduous and evergreen trees. *Remote Sensing of Environment*, *233*, 111407. https://doi.org/10.1016/j.rse.2019.111407

Wulder, M. A., Loveland, T. R., Roy, D. P., Crawford, C. J., Masek, J. G., Woodcock, C. E., et al. (2019). Current status of Landsat program, science, and applications. *Remote Sensing of Environment*, *225*, 127–147. https://doi.org/10.1016/j.rse.2019.02.015

Wutzler, T., Lucas-Moffat, A., Migliavacca, M., Knauer, J., Sickel, K., Šigut, L., et al. (2018). Basic and extensible post-processing of eddy covariance flux data with REddyProc. *Biogeosciences*, *15*(16), 5015–5030. https://doi.org/10.5194/bg-15-5015-2018

Xiao, J., Chen, J., Davis, K. J., & Reichstein, M. (2012). Advances in upscaling of eddy covariance measurements of carbon and water fluxes. *Journal of Geophysical Research*, *117*(G1), 2415. https://doi.org/10.1029/2011jg001889

Xiao, J., Chevallier, F., Gomez, C., Guanter, L., Hicke, J. A., Huete, A. R., et al. (2019). Remote sensing of the terrestrial carbon cycle: A review of advances over 50 years. *Remote Sensing of Environment*, *233*, 111383. https://doi.org/10.1016/j.rse.2019.111383

Xiao, J., Zhuang, Q., Law, B. E., Chen, J., Baldocchi, D. D., Cook, D. R., et al. (2010). A continuous measure of gross primary production for the conterminous United States derived from MODIS and AmeriFlux data. *Remote Sensing of Environment*, *114*(3), 576–591. https://doi.org/10.1016/j.rse.2009.10.013

Xiao, X., Hollinger, D., Aber, J., Goltz, M., Davidson, E. A., Zhang, Q., et al. (2004). Satellite-based modeling of gross primary production in an evergreen needleleaf forest. *Remote Sensing of Environment*, *89*(4), 519–534. https://doi.org/10.1016/j.rse.2003.11.008

Xu, K., Metzger, S., & Desai, A. R. (2017). Upscaling tower-observed turbulent exchange at fine spatio-temporal resolution using environmental response functions. *Agricultural and Forest Meteorology*, *232*, 10–22. https://doi.org/10.1016/j.agrformet.2016.07.019

Xu, X., Zhou, G., Du, H., Mao, F., Xu, L., Li, X., & Liu, L. (2020). Combined MODIS land surface temperature and greenness data for modeling vegetation phenology, physiology, and gross primary production in terrestrial ecosystems. *The Science of the Total Environment*, *726*, 137948. https://doi.org/10.1016/j.scitotenv.2020.137948

Xue, J., Anderson, M. C., Gao, F., Hain, C., Yang, Y., Knipper, K. R., et al. (2021). Mapping daily evapotranspiration at field scale using the harmonized Landsat and Sentinel-2 dataset, with Sharpened VIIRS as a Sentinel-2 thermal proxy. *Remote Sensing*, *13*(17), 3420. https://doi.org/10.3390/rs13173420

Zhang, Y., Xiao, X., Wu, X., Zhou, S., Zhang, G., Qin, Y., & Dong, J. (2017). A global moderate resolution dataset of gross primary production of vegetation for 2000–2016. *Scientific Data*, *4*(1), 170165. https://doi.org/10.1038/sdata.2017.165

Zhang, Z., Zhao, L., & Lin, A. (2020). Evaluating the performance of Sentinel-3A OLCI land products for gross primary productivity estimation using AmeriFlux data. *Remote Sensing*, *12*(12), 1927. https://doi.org/10.3390/rs12121927

References From the Supporting Information

Anderson, T., & Hoffman, P. (2006). Nutrient composition of straw used in dairy cattle diets. *University of Wisconsin Extension Focus on Forage*, *8*(1)

IPCC. (2018). *Global warming of 1.5°C: An IPCC special report on the impacts of global warming of 1.5°C above pre-industrial levels and related global greenhouse gas emission pathways, in the context of strengthening the global response to the threat of climate change, sustainable development, and efforts to eradicate poverty*. In V. Masson-Delmotte, P. Zhai, H. O. Portner, D. Roberts, J. Skea, P. R. Shukla, et al. (Eds.). IPCC.

Ishler, V. A., Adams, R. S., Heinrichs, A. J., Varga, G. A., & Concentrates for dairy cattle. (1994). Dairy and Animal Science Circular DAS, 94–06, (pp. 1–16). Retrieved from https://animalscience.psu.edu

Kathrin, H., Stefanie, B., Omta Onno, S. W. F., & Hans-Werner, O. (2017). Eco-innovations in the German fertilizer supply chain: Impact on the carbon footprint of fertilizers. *Plant Soil and Environment*, *63*(12), 531–544. https://doi.org/10.17221/499/2017-pse

NRA, CIRAD, & AFZ. (2002). *The INRA-CIRAD-AFZ Tables: Composition and nutritive values of feeds for cattle, sheep, goats, pigs, poultry, rabbits, horses and salmonids*. INRA.